

# Data-driven model reduction, Wiener projections, and the Mori-Zwanzig formalism

Kevin K. Lin

Fei Lu<sup>†</sup>

May 17, 2022

## Abstract

First-principles models of complex dynamic phenomena often have many degrees of freedom, only a small fraction of which may be scientifically relevant or observable. Reduced models distill such phenomena to their essence by modeling only relevant variables, thus decreasing computational cost and clarifying dynamical mechanisms. Here, we consider data-driven model reduction for nonlinear dynamical systems without sharp scale separation. Motivated by a discrete-time version of the Mori-Zwanzig projection operator formalism and the Wiener filter, we propose a simple and flexible mathematical formulation based on *Wiener projection*, which decomposes a nonlinear dynamical system into a component predictable by past values of relevant variables and its orthogonal complement. Wiener projection is equally applicable to deterministic chaotic dynamics and randomly-forced systems, and provides a natural starting point for systematic approximations. In particular, we use it to derive NARMAX models from an underlying dynamical system, thereby clarifying the scope of these widely-used tools in time series analysis. We illustrate its versatility on the Kuramoto-Sivashinsky model of spatiotemporal chaos and a stochastic Burgers equation.

## Contents

<b>1</b>	<b>Introduction</b>	<b>2</b>
<b>2</b>	<b>Data-driven model reduction in discrete time</b>	<b>2</b>
2.1	Setting and overview . . . . .	2
2.2	Discrete-time Mori-Zwanzig formalism . . . . .	2
2.3	NARMAX modeling . . . . .	4
<b>3</b>	<b>Wiener projections</b>	<b>4</b>
3.1	Definition and basic properties . . . . .	4
3.2	Properties of the Wiener projection . . . . .	5
3.3	Deriving NARMAX via rational approximations . . . . .	6
3.4	Parameter estimation and noise model . . . . .	6
3.5	Random dynamical systems and systems with delays . . . . .	7
<b>4</b>	<b>Numerical implementation</b>	<b>8</b>
4.1	Reformulation in cascade form . . . . .	8
4.2	Initializing and running cascade-form models . . . . .	9
4.3	Fitting models to data . . . . .	10
<b>5</b>	<b>Examples</b>	<b>11</b>
5.1	Kuramoto-Sivashinsky (KS) PDE . . . . .	11
5.2	Stochastically-forced Burgers equation . . . . .	14
<b>6</b>	<b>Concluding discussion</b>	<b>15</b>
<b>A</b>	<b>Kuramoto-Sivashinsky equation</b>	<b>19</b>
<b>B</b>	<b>Stochastic Burgers equation</b>	<b>22</b>

Department of Mathematics, University of Arizona, Tucson, AZ 85721, USA (klin@math.arizona.edu)

<sup>†</sup>Department of Mathematics, Johns Hopkins University, Baltimore, MD 21218, USA (feilu@math.jhu.edu)

## 1 Introduction

Unsteady fluid flow, fluctuations in power grids, neural activity in the brain: these and many other complex dynamical phenomena arise from the interaction of a large number of degrees of freedom across many orders of magnitude in space and time. But, in these and many other systems, only a relatively small subset of the dynamical variables are of direct interest or even observable. Reduced models, i.e., models that use only relevant dynamical variables to reproduce interesting dynamical features on relevant timescales, are thus of great potential utility, especially in tasks requiring repeated model runs like uncertainty quantification, optimization, and control. Moreover, relevant dynamical mechanisms are often easier to glean and understand in reduced models.

Many analytical and computational approaches to model reduction (also known as the “closure problem”) have been proposed, particularly in situations with sharp scale separation; see, e.g., [1, 2, 3, 4]. However, many scientific and engineering applications do not exhibit sharp scale separation, and reduced models must account for memory and noise effects [5, 6]. Moreover, while reduced models may be analytically derived in some situations, model reduction from first principles is challenging in general. This motivated much recent work on data-driven model reduction, i.e., fitting reduced models to data generated by either simulating the full model or from physical measurements; see, e.g., [7, 8, 9, 10, 11, 12].

This paper has two primary aims. First, using ideas from statistical mechanics and signal processing, we propose a simple mathematical formulation of data-driven model reduction based on a construction we call “Wiener projection.” Our formulation offers a unifying perspective on a number of model reduction strategies, and can serve as a starting point for systematic approximations in model reduction. Second, we show that a version of the NARMAX (Nonlinear Auto-Regressive Moving Average with eXogenous input) representation of stochastic processes, widely used in time series analysis and modeling (see [13, 14, 8] and references therein), can be derived via Wiener projections. We show that Wiener projections are equally applicable to deterministic chaotic dynamics and randomly-forced systems, and illustrate its versatility on the Kuramoto-Sivashinsky model of spatiotemporal chaos and a viscous Burgers equation with stochastic forcing.

## 2 Data-driven model reduction in discrete time

### 2.1 Setting and overview

We assume the full system of interest is a discrete-time dynamical system

$$X_{n+1} = F(X_n). \quad (2.1)$$

The states  $X_n$  are points in a space  $\mathbb{X}$ , which can be a vector space or more general manifold. We refer to Eq. (2.1) as the *full model*. The dynamical variables of interest, or *relevant variables*, are defined by  $x = \pi(X)$ ,  $\pi$  being a given function mapping points in  $\mathbb{X}$  to points in  $d$ -dimensional Euclidean space  $\mathbb{R}^d$ , generally with  $d \ll \dim(\mathbb{X})$ . Eq. (2.1) can accommodate continuous time systems by letting  $F$  be the time- $\Delta t$  solution map (for some  $\Delta t > 0$ ) or a Poincaré map. We focus on discrete-time reduction because (i) observations are always discrete in time, and (ii) discrete-time reduced models avoid the numerical errors that come from integrating continuous time reduced models, which can be significant in chaotic systems [8, 15].

We want reduced models that use only the relevant variables and are capable of (i) forecasting  $x_n$  given its past history, and (ii) reproducing long-time statistics, e.g., correlations and marginal distributions. In general, parametric model reduction methods begin with a family of models with unknown parameters  $\alpha = (\alpha_1, \alpha_2, \dots, \alpha_v)$  and observations  $\tilde{x}_n = \pi(\tilde{X}_n)$ , where  $(\tilde{X}_n)_{n=0}^N$  is a trajectory of the full model. One then chooses  $\alpha$  by fitting the model to the data, usually by minimizing a suitable loss function. Methods differ in their choice of models and loss function, which can impact both model fitting and the performance of the reduced model.

### 2.2 Discrete-time Mori-Zwanzig formalism

The MZ formalism originally arose in classical statistical mechanics [6, 16], and has been used in physical applications ranging from fluid dynamics to materials science and molecular dynamics (see, e.g., [5, 17, 10, 18, 19, 20, 21, 22, 23, 24, 25, 26]). As explained in Sect. 3.5, it also applies to systems with random forcing and/or (bounded) delays. Here we review a discrete MZ theory; see also Darve *et al.* [27].

In MZ theory, one views the space of observables on  $\mathbb{X}$  as forming a Hilbert space  $\mathbb{H}$  with inner product  $\langle f, g \rangle = \int f g \, d\mu$ . The probability distribution  $\mu$  describes the long-time statistics of typical solutions of Eq. (2.1), and is *invariant*, i.e., if  $X_0$  has distribution  $\mu$ , then so does  $X_n$  for all  $n > 0$ . Inner products are thus naturally interpreted as steady-state correlations. The choice of  $\mu$  depends on the setting: for Hamiltonian systems, one

often uses canonical or microcanonical ensembles; for dissipative chaotic systems, singular distributions on strange attractors are often appropriate. For simplicity, we assume  $X_0$  has distribution  $\mu$ , so that  $(X_n)$  is stationary.

To reformulate the dynamics on  $\mathbb{H}$  and produce a reduced model, let  $M$  be the *Koopman operator*  $M\varphi(X) = \varphi(F(X))$  and  $P$  a projection operator on  $\mathbb{H}$  whose range  $\mathbb{V}$  are functions that depend *only* on the relevant variables  $x$ . (The Koopman operator advances observables forward in time:  $M\varphi(X)$  gives the value of  $\varphi$  at the next step if the current state is  $X$ .) The *Mori-Zwanzig equation* then asserts that there exists a sequence of functions  $\xi_1, \xi_2, \dots$ , such that for  $n \geq 0$ ,

$$x_{n+1} = PF(x_n) + \sum_{k=1}^n \Gamma_k(x_{n-k}) + \xi_{n+1}(X_0) \quad (2.2)$$

with  $\Gamma_k = P(\xi_k \circ F)$  and  $P\xi_n = 0$ . The first, “Markov” term in Eq. (2.2) is the best approximation of  $F$  by functions in  $\mathbb{V}$ . The second, “memory” term captures all non-Markovian effects representable in  $\mathbb{V}$ . The last, “noise” term represents errors at each step, and are uncorrelated with functions in  $\mathbb{V}$ . Eq. (2.2) follows from the *Dyson formula*

$$M^{n+1} = \sum_{k=0}^n M^{n-k} PM(QM)^k + (QM)^{n+1}, \quad (2.3)$$

where  $Q = I - P$  is the orthogonal projection. Applying both sides to  $\pi$  and defining  $\xi_n = (QM)^n \pi$  yields Eq. (2.2). See Sect. 4 for details.

A simple choice of  $P$  is to fix a collection of linearly independent functions  $\psi_1(x), \dots, \psi_\nu(x)$  of  $x$ , then take  $P$  to be orthogonal projection onto their linear span, i.e.,

$$P\varphi(x) = \Psi(x) \cdot \langle \Psi, \Psi \rangle^{-1} \cdot \langle \Psi, \varphi \rangle, \quad (2.4)$$

where  $\langle f, g \rangle = \int f^T \cdot g \, d\mu$  for matrix-valued  $f$  and  $g$ , and the columns of  $\Psi(x) = [\psi_1(x) \ \dots \ \psi_\nu(x)]$  span  $\mathbb{V}$ . See, e.g., [5, 28, 6, 18] for discussions of other common choices, e.g., the conditional expectation  $(P\varphi)(x) = \mathbb{E}_\mu(\varphi(X)|\pi(X) = x)$ .

With  $P$  as in Eq. (2.4), we can write  $PF = \Psi \cdot h_0$  and  $\Gamma_k = \Psi \cdot h_k$  for coefficient vectors  $h_k$ . Eq. (2.2) then becomes

$$x_{n+1} = \sum_{k \geq 0} \Psi(x_{n-k}) \cdot h_k + \xi_{n+1}, \quad (2.5a)$$

$$\text{with} \quad \langle \xi_n, \Psi \circ \pi \rangle = 0. \quad (2.5b)$$

To arrive at a closed equation for  $x_n$ , MZ theory typically replaces  $\xi_n$  by, e.g., a stationary Gaussian process, and approximates  $h_n$  by, e.g., field-theoretic perturbation theory [29, 6].

Orthogonality conditions (e.g., Eq. (2.5b)) play a key role in MZ theory and in Wiener filtering (Sect. 3): they are equivalent to optimality in the least squares sense. Furthermore, in using reduced models to generate predictions, one often assumes the driving noise  $\xi_n$  is independent of  $x_m$  for  $n > m$ . Orthogonality conditions provide partial justification for this (standard) procedure. Eq. (2.5b) comes from  $P\xi_n = 0$ , but does *not* imply  $\Psi(x_m)$  is uncorrelated with  $\xi_n$  for  $n > m$ . More on this in Sect. 3.

*Deriving the Mori-Zwanzig equation from the Dyson formula.* In the above, we asserted that for any projection operator  $P$ , the Mori-Zwanzig equation Eq. (2.2) follows from the Dyson formula Eq. (2.3). (In the above,  $Q = I - P$  is the orthogonal projection, so that  $P\xi_n = 0$  for  $n > 0$ .) To see this, apply both sides of Eq. (2.3) to the observation function  $\pi$  and evaluate at  $X_0$ , yielding

$$\underbrace{(M^{n+1}\pi)(X_0)}_{(I)} = \underbrace{\sum_{k=0}^n (M^{n-k}PM(QM)^k\pi)(X_0)}_{(II)} + \underbrace{((QM)^{n+1}\pi)(X_0)}_{(III)}. \quad (2.6)$$

For Term (I), the definition of the Koopman operator  $M$  gives  $\pi(F^{n+1}(X_0)) = \pi(X_{n+1}) = x_{n+1}$ . For Term (III), we have (by definition)  $\xi_{n+1}(X_0)$ . For Term (II), we have

$$(M^{n-k}PM(QM)^k\pi)(X_0) = (PM(QM)^k\pi)(X_{n-k})$$

as before. Since  $M(QM)^k\pi = M\xi_k = \xi_k \circ F$  and the range of  $P$  consists of functions of  $x = \pi(X)$ , we get

$$(M^{n-k}PM(QM)^k\pi)(X_0) = P(\xi_k \circ F)(x_{n-k}).$$

Combining all these and  $PQ = 0$  yields Eq. (2.2).

### 2.3 NARMAX modeling

Whereas MZ theory seeks systematic derivations of reduced models, NARMAX (Nonlinear Auto-Regressive Moving Average with eXogenous input) is a generic approach to parametric data-driven modeling of stationary time series [30, 13, 14]. A common version of the NARMAX model is

$$x_{n+1} = f(x_n) + z_n, \quad (2.7a)$$

$$\begin{aligned} z_n + a_{p-1}z_{n-1} + \dots + a_0z_{n-p} &= d_q\eta_n + \dots + d_0\eta_{n-q} \\ &\quad + \Psi(x_n) \cdot c_1 + \dots + \Psi(x_{n-r}) \cdot c_r, \end{aligned} \quad (2.7b)$$

where  $f$  and  $\Psi$  are given functions, and the  $\eta_i$  are independent, identically-distributed (IID) random variables, often Gaussian for simplicity. One can view  $x_{n+1} = f(x_n)$  as a crude predictor of  $x_{n+1}$ , and Eq. (2.7b) a corrector based on a model of the residuals  $z_n$ . In applications, the would-be modeler chooses the forms of  $f$  and  $\Psi$  and the orders  $p, q, r$ , then determines  $a_i, c_i$ , and  $d_i$  by minimizing a suitable loss function. Note that like the MZ equation, Eq. (2.7) is non-Markovian.

## 3 Wiener projections

### 3.1 Definition and basic properties

As mentioned in Sect. 2.2, the MZ equation (2.5) does not guarantee all desired orthogonality relations. To fix this, we first recall the idea of Wiener filters [31, 32]: let  $u_n$  and  $v_n$  be two zero-mean wide-sense stationary processes. The Wiener filter ( $h_n$ ) minimizes the mean-squared error (MSE):

$$\mathbb{E}(\|u_n - (v \star h)_n\|^2), \quad (3.1)$$

where  $(v \star h)_n = \sum_k v_{n-k} \cdot h_k$  denotes convolution, with  $h_n = 0$  for  $n < 0$ . It satisfies the orthogonality condition

$$\text{cov}(v_m, w_n) = 0, \quad n \geq m, \quad (3.2)$$

where  $w_n$  is the residual  $u_n - \sum_k v_{n-k} \cdot h_k$ , i.e., filter errors are uncorrelated with the data on which filter output is based. Eq. (3.2) is equivalent to the minimum-MSE criterion, and ensures the total power in  $(x_n)$  does not exceed that of  $(X_n)$ .

We observe that the Wiener filter can be applied to model reduction as well: with  $X_n$  as in Eq. (2.1) and  $\Psi$  as before, let  $h_n$  be the causal Wiener filter for  $u_n = x_{n+1} = \pi(X_{n+1})$  and  $v_n = \Psi(x_n)$ . We then obtain  $x_{n+1} = \sum_{k \geq 0} \Psi_{n-k} \cdot h_k + \xi_{n+1}$  with  $\text{cov}(\Psi(x_m), \xi_n) = 0$  for  $n > m$  with  $\xi_n$  playing the role of the residual  $w_n$  in Eq. (3.2). This is very similar to Eq. (2.5a) but with stronger orthogonality guarantees than Eq. (2.5b).

We now sketch an argument showing that Wiener-based model reduction is in fact a special case of the MZ equation. (Assumptions and details in Sect. 3.2.) To see this, let  $\Psi_n = \Psi(x_n)$ , and assume  $F$  is invertible (as when  $F$  is the time- $T$  or Poincaré map of a differential equation) so that  $M$  is also invertible. Let  $P_W$  be orthogonal projection onto the subspace

$$W = \text{span}(\Psi \cup M^{-1}\Psi \cup M^{-2}\Psi \cup \dots), \quad (3.3)$$

where  $M^{-k}\Psi$  is a short-hand for  $\{M^{-k}\psi_1, \dots, M^{-k}\psi_\nu\}$ . Since  $M^{-1}v \in W$  for all  $v \in W$ , we have

$$M^{-\ell}P_W = P_W M^{-\ell}P_W, \quad \ell \geq 0. \quad (3.4)$$

With this, the Dyson formula (2.3) simplifies to

$$M^{n+1} = M^n P_W M + (Q_W M)^{n+1}. \quad (3.5)$$

Applying both sides of Eq. (3.5) to  $\pi$ , we obtain (see Sect. 3.2)

$$x_{n+1} = \sum_{k \geq 0} \Psi(x_{n-k}) \cdot h_k + \xi_{n+1}, \quad (3.6a)$$

$$\langle \xi_n, \Psi_m \rangle = 0 \text{ for } n > m. \quad (3.6b)$$

Though Eq. (3.6a) and Eq. (2.5a) are formally identical, the orthogonality relation (3.6b) is strictly stronger than Eq. (2.5b). In addition, one can show that the Wiener projection guarantees the joint wide-sense stationarity of  $x_n$ ,  $\xi_n$ , and  $\Psi_n$ ; see Sect. 3.2. We refer to the projection  $P_W$  and the associated decomposition (3.6) as the *Wiener projection*.

### 3.2 Properties of the Wiener projection

In the above, we claimed that the Wiener projection  $P_W$  has the following properties:

- (i) Eq. (3.4) implies the existence of  $h_0, h_1, \dots$  such that Eqs. (3.6) hold. Furthermore, if the vectors  $\cup_{k \geq 0} M^{-k} \Psi$  are linearly independent, then the coefficients  $(h_k)$  are unique.
- (ii) The correlation matrices  $\langle \xi_m, \Psi_n \rangle$  and  $\langle \xi_m, \xi_n \rangle$  are functions of  $m - n$ , i.e.,  $\xi_m$  and  $\Psi_n$  are jointly wide sense stationary. (The process  $(\Psi_n)$  is stationary by assumption.)

We now justify these claims. We assume the full model  $F$  to be invertible, so that the Koopman operator  $M$  is also invertible, with  $M^{-1}\varphi = \varphi \circ F^{-1}$ . One can show that the Koopman operator is unitary (i.e.,  $MM^* = M^*M = I$ ) and  $P_W$  self-adjoint ( $P_W = P_W^*$ ), where  $L^*$  denotes the adjoint of an operator  $L$  on the Hilbert space  $\mathbb{V}$  of observables with the inner product  $\langle f, g \rangle = \int fg d\mu$ ; see Sect. 2.2 for definitions and, e.g., [33] for relevant background.

To establish Eq. (3.5), apply the Dyson formula Eq. (2.3) to the projection  $P_W$ :

$$M^{n+1} = \sum_{k=0}^n M^{n-k} P_W M (Q_W M)^k + (Q_W M)^{n+1}. \quad (3.7)$$

We claim the terms with  $k \geq 1$  disappear, so that we have Eq. (3.5). First, notice the subspace  $W$  is (backward) invariant in the sense that for all vectors  $v \in W$ , we have  $M^{-1}v \in W$ . This implies Eq. (3.4), which in turn implies  $P_W M^k Q_W M = P_W M^k P_W Q_W M = 0$ . So  $M^{n-k} P_W M (Q_W M)^k = 0$  for  $k = 1, 2, \dots, n$ , and the Dyson formula simplifies to Eq. (3.5). Applying both sides of Eq. (3.5) to  $\pi$ , we have Eq. (3.6a). The orthogonality Eq. (3.6b) follows from the fact that  $P_W$  is an orthogonal projection and the definition of the space  $W$ . Uniqueness is straightforward if  $\cup_{k \geq 0} \{M^{-k} \Psi\}$  is linearly independent.

Next, we show that  $\xi_n = (Q_W M)^n \pi$  is wide sense stationary. First, by taking adjoints in Eq. (3.4), we get  $P_W M^\ell = P_W M^\ell P_W$ . A short calculation yields

$$M^\ell Q_W = Q_W M^\ell Q_W, \quad \ell \geq 0. \quad (3.8)$$

Repeated applications of Eq. (3.8) with  $\ell = 1$  leads to

$$(Q_W M)^n \pi = M^{n-1} Q_W M \pi \quad (3.9a)$$

$$= M^{n-1} \xi_1 \quad (3.9b)$$

$$= \xi_1 \circ F^{n-1}, \quad n = 1, 2, \dots \quad (3.9c)$$

Thus,  $\langle \xi_m, \xi_n \rangle = \langle \xi_1 \circ F^{m-1}, \xi_1 \circ F^{n-1} \rangle$ . Since the probability distribution  $\mu$  is invariant for  $F$ , we have

$$\begin{aligned} \langle \xi_1 \circ F^{m-1}, \xi_1 \circ F^{n-1} \rangle &= \int \xi_1(F^{m-1}(x)) \cdot \xi_1(F^{n-1}(x))^T d\mu(x) \\ &= \int \xi_1(F^{m-n}(x)) \cdot \xi_1(x)^T d\mu(x) \\ &= \langle \xi_1 \circ F^{m-n}, \xi_1 \rangle, \end{aligned}$$

i.e.,  $\xi_1, \xi_2, \dots$  is wide sense stationary.

To see that  $\langle \xi_m, \Psi_n \rangle$  is also a function of  $m - n$ , observe

$$\langle \xi_m, \Psi_n \rangle = \langle \xi_1 \circ F^{m-1}, \Psi_0 \circ F^n \rangle \quad (3.10a)$$

$$= \langle \xi_1 \circ F^{m-n-1}, \Psi_0 \rangle, \quad (3.10b)$$

using Eq. (3.9) and the invariance of  $\mu$ .

*Remarks.*

- (i) The lack of memory terms in Eq. (3.5) is not surprising: we have simply incorporated all relevant memory effects in the definition of  $P_W$  itself, and also assumed the availability of that entire past history at the initial time  $n = 0$ , so there is nothing more for a memory term to capture. However, one only has a finite amount of memory in practice. With approximations like NARMAX, this means the corresponding projection  $\tilde{P}_W$  would not satisfy Eq. (3.7) exactly, and there will again be memory terms. One expects these terms to become smaller as the the approximation  $\tilde{P}_W$  is improved; a detailed analysis is left for future work.

- (ii) Though  $W$  is defined in terms of  $M^{-1}$  and its powers, in practice one does not need to compute  $M^{-1}$  or  $F^{-1}$  in working with  $W$  as one can simply keep track of the (recent) history in stepping forward the reduced model. So our formalism can be safely applied to dissipative dynamical systems, for which  $F^{-1}$  may be extremely unstable.
- (iii) More “operator-theoretic” arguments can also be given for many of the above results. For example, the joint stationarity of  $\xi_n$  and  $\Psi_m$  follows from

$$P_W M^{-m} (Q_W M)^n = P_W M^{-m} M^{n-1} Q_W M \quad (3.11a)$$

$$= P_W M^{n-m-1} Q_W M. \quad (3.11b)$$

(Eq. (3.11a) follows by repeated use of Eq. (3.8) with  $\ell = 1$ .) When  $n > m$ , Eq. (3.8) implies the last line is 0, which implies the orthogonality Eq. (3.6b).

### 3.3 Deriving NARMAX via rational approximations

Eq. (3.6) would not reduce computational cost unless the sum in  $k$  can be truncated. Simply keeping a small number of terms, however, may not provide a good approximation. Put another way, to use Eq. (3.6) as the basis for model reduction, it is necessary to find an effective way to parametrize the space of filters ( $h_n$ ). To handle this, we use an idea from MZ theory [6]: let  $x_n$ ,  $\psi_n$ ,  $h_n$ , and  $\xi_n$  be (possibly matrix-valued) zero-mean wide-sense stationary time series satisfying  $x_{n+1} = \sum_{k \geq 0} \psi_{n-k} \cdot h_k + \xi_n$ , with  $\text{cov}(x_m, \xi_n) = \text{cov}(\psi_m, \xi_n) = 0$  for all  $m, n$ . Let  $H(z) = \sum_{n \geq 0} h_n z^{-n}$  denote the  $z$ -transform of  $h_n$ , and  $S_{\varphi\eta}(\theta) = \sum_n C_{\varphi\eta}(n) e^{in\theta}$  the spectral power density associated with  $C_{\varphi\eta}(n) = \text{cov}(\varphi(X_n), \eta(X_n))$ . Then

$$S_{xx}(\theta) = |H(e^{i\theta})|^2 S_{\psi\psi}(\theta) + S_{\xi\xi}(\theta). \quad (3.12)$$

In MZ theory, rational approximations of transfer functions (e.g.,  $H(z)$ ) are frequently very effective [6]. This suggests we take  $H(z) \approx B(z)/A(z)$ , with  $B(z) = b_q z^q + \dots + b_0$  and  $A(z) = z^p + a_{p-1} z^{p-1} + \dots + a_0$ . Applying this to Eq. (3.6) and rearranging yields

$$x_{n+1} = y_n + \xi_{n+1}, \quad (3.13a)$$

$$y_n + a_{p-1} y_{n-1} + \dots + a_0 y_{n-p} = \Psi_{n-p+q} \cdot b_q + \dots + \Psi_{n-p} \cdot b_0. \quad (3.13b)$$

If we set one column of  $\Psi$  to be  $f$  in Eq. (2.7) and approximate the noise by  $\xi_n \approx d_q \eta_n + \dots + d_0 \eta_{n-q}$ , Eq. (3.13) is essentially Eq. (2.7). Thus, in seeking to derive a practical reduced model based on Eq. (3.6), we have arrived at a version of NARMAX.

Eq. (3.13) is equivalent to the multistep recursion

$$x_{n+p+1} + a_{p-1} x_{n+p} + \dots + a_0 x_{n+1} = \Psi_{n+q} \cdot b_q + \dots + \Psi_n \cdot b_0 + \bar{\xi}_{n+1}, \quad (3.14)$$

where  $\bar{\xi} = a * \xi$ . This is another way to write the NARMAX model. Unlike Eq. (3.13), this formulation does not introduce any auxiliary variables. The noise ( $\bar{\xi}_n$ ) in Eq. (3.14) is related to the ( $\xi_n$ ) in Eq. (3.13) by  $S_{\bar{\xi}\bar{\xi}}(\theta) = |A(e^{i\theta})|^2 S_{\xi\xi}(\theta)$ . This means there is no simple orthogonality relation between  $\bar{\xi}_n$  and  $\Psi_n$ . For these reasons, Eq. (3.14) is slightly less convenient than Eq. (3.13) for model fitting. Both require  $p$  vectors of length  $d$  as initial conditions.

### 3.4 Parameter estimation and noise model

The preceding considerations suggest a simple, two-step approach parametric model reduction, based on Eq. (3.13). The first step is to determine the coefficients  $a_i$  and  $b_i$ . We do this by minimizing the *one-step prediction error*  $\sum_{n=p}^{N-1} \|\tilde{x}_{n+1} - \hat{x}_{n+1}\|^2$ , where  $(\tilde{x}_n)$  are observations from the full model and  $\hat{x}_{n+1}$  are predictions of  $x_{n+1}$  based on  $\tilde{x}_n, \tilde{x}_{n-1}, \dots$ , computed from

$$\hat{x}_{n+1} = \sum_{k=0}^n \Psi(\tilde{x}_{n-k}) \cdot h_k; \quad (3.15)$$

modulo transients, this is Eq. (3.6) with  $\Psi_n = \Psi(\tilde{x}_n)$  and  $\xi_n \equiv 0$ . In practice, we use a version of Eq. (3.13) for efficient, stable computation of  $\hat{x}_n$ ; see Sect. 4 for details.

For Eq. (3.6) to be meaningful, we need  $h_n \rightarrow 0$ . With  $H(z) \approx B(z)/A(z)$ , this decaying memory condition is guaranteed if the roots of  $A(z)$  lie strictly inside the unit circle. This highly-nonlinear constraint becomes linear if one rewrites the  $p$ th-order system (3.13) as a cascade of first- and second-order systems, at the cost of trading a quadratic loss function for a nonconvex one; see Sect. 4. Note the decaying memory condition, known in the engineering literature as “bounded-input bounded-output stability,” is necessary but not sufficient for the overall numerical stability of the reduced model.

After finding optimal values for  $a_i$ ,  $b_i$ , and the initial  $y_i$ , we fit a stationary Gaussian process to the residuals  $\tilde{\xi}_{n+1} = \tilde{x}_{n+1} - \tilde{x}_{n+1}$  by estimating its power spectrum via averaging multiple periodograms, then sampling  $\xi_n$  by a random Fourier series; see, e.g., [34] and references therein. More efficient and accurate methods are available [35]; moving average representations (see, e.g., [8]) can also be used. Whatever the method, the resulting reduced models will only satisfy the orthogonality conditions approximately. We have found our procedure to be effective when  $(\xi_n)$  are relatively small, as occurs in many applications.

Finally, we point out that the parameter estimator described above is very much guided by the theory of wide sense stationary processes. An alternative, based on maximum likelihood estimation of NARMAX models, was developed and used in [8, 36]. In conjunction with [36], the example in Sect. 5.1 lets us compare the two.

### 3.5 Random dynamical systems and systems with delays

Model reduction techniques are routinely applied to both deterministic and random dynamical systems, as well as systems with delays. The MZ formalism applies to both random dynamical systems and to discrete-time systems with bounded delays, as we now explain.

We first explain how the MZ formalism applies to random dynamical systems. To simplify notation, we do this in the context of the discretized stochastic Burgers equation

$$u_k^{n+1} = G_k(u^n, \Delta t) + \sqrt{\Delta t} \sigma_k w_k^n, \quad k = 1, \dots, K. \quad (3.16)$$

To simplify notation, let  $u^n = (u_1^n, \dots, u_K^n)$  and  $w^n = (w_1^n, \dots, w_K^n)$  denote the state and forcing at time  $n$ , respectively. Then the above has the general form

$$u^{n+1} = F(u^n, w^n). \quad (3.17)$$

Let  $\underline{w} = (\dots, w^{-1}, w^0, w^1, \dots)$  denote the entire history of the forcing. A standard way to rewrite Eq. (3.16) as an autonomous dynamical system (Eq. (2.1) above) is to augment the state  $u^n$  with the history of the forcing  $\underline{w}$ . In dynamical systems language, such constructions are known as “skew products.” Here we sketch the key ideas, and refer interested readers to, e.g., [37, 38, 39] for mathematical details (see also [40, 41] for extensions to stochastic differential equations).

Given a forcing sequence  $\underline{w}$ , we define  $\sigma(\underline{w})$  to be the sequence whose  $n$ th entry is  $w^{n+1}$ , i.e.,  $\sigma(\underline{w})^n = w^{n+1}$ . In other words,  $\sigma(\underline{w})$  is sequence  $\underline{w}$  shifted by 1 in time. If we shift  $n$  times, then  $w^n$  is moved into position 0, so that  $(e_0(\sigma^n(\underline{w}))) = w^n$ , where  $e_0(\underline{w}) = w^0$ .

Using this notation, we can rewrite Eq. (3.17) as  $u^{n+1} = F(u^n, e_0(\sigma^n(\underline{w})))$ , where  $\underline{w}$  is a given realization of the forcing sequence. Now denote  $\underline{w}^{(n)} = \sigma^n(\underline{w})$ ; then  $\{\underline{w}^{(n)} \mid n \in \mathbb{Z}\}$  is a sequence of forcing sequences, all related to each other by time shifts. Then

$$u^{n+1} = F(u^n, e_0(\underline{w}^{(n)})), \quad (3.18a)$$

$$\underline{w}^{(n+1)} = \sigma(\underline{w}^{(n)}). \quad (3.18b)$$

Let  $\mathbb{X}$  be the space of all pairs  $(u, \underline{w})$ , i.e.,  $\mathbb{X}$  is the state space of the discretized Burgers equation augmented with its forcing history. Then Eq. (3.18) is a dynamical system of the form Eq. (2.1), albeit one with an infinite-dimensional state space  $\mathbb{X}$ . This does not prevent one from applying the Mori-Zwanzig formalism. In practice, one also does not need to keep track of the entire forcing history  $\underline{w}$ , just a fragment of it. Note that within this framework, observation functions  $\Psi$  can depend on both the state  $u^n$  and the forcing history  $\underline{w}^{(n)}$ .

Finally, we note that an invariant probability distribution  $\mu$ , related in a natural way to the stationary distribution of Eq. (3.16), can be constructed on this augmented state space. We do not do this here; interested readers are referred to, e.g., [37].

As for general delay terms, for example terms of the form  $\Psi(x_k, x_{k-\ell})$  for  $\ell \leq L$  (which are used in our model for the Burgers equation, one can use a standard construction: as in Eq. (2.1), let  $F$  be a given dynamical system

with state space  $\mathbb{X}$ , and replace the state space  $\mathbb{X}$  by the  $(L + 1)$ -fold cartesian product  $\overline{\mathbb{X}} = \mathbb{X}^{L+1}$ , and replace  $F$  by a map  $\overline{F}$  on  $\overline{\mathbb{X}}$  with

$$\overline{F}(\overline{X}) = \overline{F}(X_0, \dots, X_L) = (F(X_0), X_0, \dots, X_{L-1}) \quad (3.19)$$

for  $\overline{X} = (X_0, \dots, X_L) \in \overline{\mathbb{X}}$ . This constructions can be combined with the skew product construction described earlier to handle stochastic systems with delays.

## 4 Numerical implementation

As mentioned in Sect. 3, one of the issues in fitting a model of the form Eq. (3.6) to data is enforcing the decaying memory condition  $h_k \rightarrow 0$  in Eq. (3.6). Here we describe one approach to enforcing this condition and an accompanying algorithm for fitting reduced models to time series data, which we have found to be effective for the examples in this paper. Note that more efficient algorithms are possible using, e.g., power spectra estimates. These possibilities are studied in upcoming work.

First, recall the representation (Eq. (3.13) in Sect. 3.3, which implements Eq. (3.6a) with a rational transfer function  $H(z) = B(z)/A(z)$ . Following the MZ and Wiener formalisms, we seek coefficients  $a = (a_0, \dots, a_{p-1})$  and  $b = (b_0, \dots, b_q)$  that minimize

$$\mathcal{E}(a, b) = \frac{1}{N} \sum_{n=0}^{N-1} \left\| \tilde{x}_{n+1} - \hat{x}_{n+1}(\tilde{\Psi}_1, \dots, \tilde{\Psi}_n; a, b) \right\|^2 \quad (4.1)$$

where  $\hat{x}_{n+1}(\dots)$  is the one-step prediction Eq. (3.15), equivalently

$$\begin{aligned} \hat{x}_{n+1} &= y_n, \\ y_n + a_{p-1}y_{n-1} + \dots + a_0y_{n-p} &= \Psi(\tilde{x}_{n-p+q}) \cdot b_q + \dots + \Psi(\tilde{x}_{n-p}) \cdot b_0 \end{aligned} \quad (4.2)$$

modulo transients. It is well known (see, e.g., [31]) that in order to have  $h_n \rightarrow 0$  as  $n \rightarrow \infty$ , a causal linear filter with meromorphic transfer function  $H(z)$  must have all its poles strictly inside the unit disc  $D^1$ . With  $H(z) = B(z)/A(z)$ , this stability constraint is the same as requiring the roots of  $A(z)$  to lie strictly inside  $D^1$ .

In standard approaches to Wiener filtering, one assumes the power spectra  $S_{xx}$ ,  $S_{x\psi}$ , and  $S_{\psi\psi}$  and their meromorphic continuations to a domain in the complex plane containing  $D^1$  are available. The decaying memory constraint can then be imposed by Wiener-Hopf techniques (see, e.g., [32]). In the context of data-driven modeling, direct minimization of  $\mathcal{E}(a, b)$  is more attractive because of the various sources of statistical error. However, in terms of the coefficients  $a_i$ , the decaying memory condition is a highly nonlinear constraint. Our approach is to reformulate Eq. (3.13) so that the decaying memory constraint becomes easier to implement, though at the cost of making the cost function highly non-convex. We then fit reduced models to data using this representation by numerical optimization.

In Sects. 4.1 and 4.2 below, we describe the reformulated model, assuming model coefficients have already been determined and a suitable noise model  $\xi_n$  constructed. Sect. 4.3 explains how we infer model coefficients by numerical optimization.

### 4.1 Reformulation in cascade form

Consider a model of the form Eq. (3.13) in which the coefficients are already known, and suppose  $A(z)$  has real scalar coefficients.<sup>1</sup> Our reformulation is based on the observation that for a quadratic polynomial  $z^2 + az + \beta$ , its roots lie inside the unit disc if and only if  $(\alpha, \beta)$  lies inside the triangle in the  $\alpha\beta$ -plane with vertices  $(\pm 2, 1)$  and  $(0, -1)$ . That is to say, for such an  $A(z)$ , the decaying memory condition consists of three *linear* inequalities.

To make use of this observation for non-quadratic  $A(z)$ , we factor  $A(z)$  into a product of quadratic factors when  $p = \deg(A)$  is even, and quadratic factors and one linear factor if  $p$  is odd, i.e.,

$$A(z) = \prod_{i=1}^{p/2} (z^2 + \alpha_i z + \beta_i) \quad \text{or} \quad A(z) = (z + \alpha_0) \prod_{i=1}^{\lfloor p/2 \rfloor} (z^2 + \alpha_i z + \beta_i). \quad (4.3)$$

In this form, the decaying memory condition is naturally expressed as a system of linear inequalities, which are easily imposed when performing numerical optimization.

<sup>1</sup>This is sufficient for the examples considered in this paper, and does not entail any loss of generality if one is willing to increase the degrees and dimensions of  $A$  and  $B$ .

In view of the convolution theorem for z-transforms, the quadratic factorization of  $A(z)$  is equivalent to representing the linear filter with transfer function  $1/A(z)$  as a *cascade of second-order filters*. Suppose, for simplicity, that  $p = 2r$ . We introduce an auxiliary variable  $z_i^n$  for the  $i$ th stage in the cascade. (The auxiliary variables  $z_i^n$  differ from the  $z$  in Eq. (4.3).) Then the system

$$\begin{aligned} \text{Stage 1} \quad z_1^n + \alpha_1 z_1^{n-1} + \beta_1 z_1^{n-2} &= \Psi_{n-p+q} \cdot b_q + \cdots + \Psi_{n-p} \cdot b_0 \\ \text{Stage 2} \quad z_2^n + \alpha_2 z_2^{n-1} + \beta_2 z_2^{n-2} &= z_1^n \\ \vdots & \vdots \\ \text{Stage } r \quad z_r^n + \alpha_r z_r^{n-1} + \beta_r z_r^{n-2} &= z_{(r-1)}^n \end{aligned} \quad (4.4a)$$

with output

$$x_{n+1} = z_r^n + \xi_{n+1}. \quad (4.4b)$$

is equivalent to Eq. (3.13). The recursion in Eq. (4.4) is explicit when  $p \geq q$ . In the notation of Eq. (3.13), the output of the last stage gives  $y_n$ , i.e.,  $y_n = z_r^n$ .

One can better understand the structure of the system (4.4) by considering some specific cases. For instance, with  $p = q = 4$ , we have two stages:

$$\begin{aligned} \text{Stage 1} \quad z_1^n + \alpha_1 z_1^{n-1} + \beta_1 z_1^{n-2} &= \Psi_n \cdot b_4 + \cdots + \Psi_{n-4} \cdot b_0 \\ \text{Stage 2} \quad z_2^n + \alpha_2 z_2^{n-1} + \beta_2 z_2^{n-2} &= z_1^n \end{aligned} \quad (4.5)$$

In this case, it is easy to show directly that

$$y_n + a_3 y_{n-1} + \cdots + a_0 y_{n-4} = \Psi_n \cdot b_4 + \cdots + \Psi_{n-4} \cdot b_0 \quad (4.6)$$

where  $y_n = z_2^n$  and

$$z^4 + a_3 z^3 + a_2 z^2 + a_1 z + a_0 = (z^2 + \alpha_1 z + \beta_1) \cdot (z^2 + \alpha_2 z + \beta_2), \quad z \in \mathbb{C}. \quad (4.7)$$

The corresponding reduced model can be written as a system

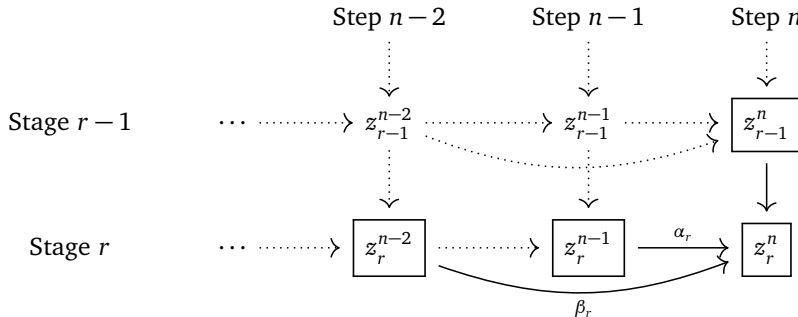
$$\begin{aligned} x_{n+1} &= y_n + \xi_{n+1} \\ y_n &= -(a_3 y_{n-1} + \cdots + a_0 y_{n-4}) + (\Psi_n \cdot b_4 + \cdots + \Psi_{n-4} \cdot b_0). \end{aligned}$$

With  $p = q = 0$ , we have a one-step (Galerkin) recursion  $x_{n+1} = \Psi_n \cdot b_0 + \xi_{n+1}$ . Similary, with  $p = q = 1$ , we have  $x_{n+1} = y_n + \xi_{n+1}$  and  $y_n = -a_0 y_{n-1} + \Psi_n \cdot b_1 + \Psi_{n-1} \cdot b_0$ , and setting  $a_0 = 0$  yields  $x_{n+1} = \Psi_n \cdot b_1 + \Psi_{n-1} \cdot b_0 + \xi_{n+1}$ .

## 4.2 Initializing and running cascade-form models

Running the model to produce predictions entails carrying out the recursions in Eq. (4.4), at each point computing the predictors  $\Psi_n = \Psi(x_n)$  with  $x_n = y_{n-1} + \xi_n = z_r^{n-1} + \xi_n$ . Though derived from Eq. (3.13), Eq. (4.4) is quite different in form. Here we examine Eq. (4.4) more closely, to clarify the flow of information in the algorithm and other details.

It is useful to first visualize Eq. (4.4) as a computation graph, a fragment of which is shown here:



(For legibility, we have drawn the edges going into  $z_r^n$  as solid lines; all others are dotted.) The variable  $z_r^n$  at time  $n$  and stage  $r$  depends on the corresponding variable  $z_{r-1}^n$  in the previous stage, as well as the two previous steps ( $z_r^{n-1}$  and  $z_r^{n-2}$ ) in the same stage.

Once we have initial conditions, Eq. (4.4) can be iterated to generate sample paths. The first thing is then to find the initial values  $z_i^{p-1}$  and  $z_i^{p-2}$  for  $i = 1, \dots, r$  from the given data  $\tilde{x}_1, \dots, \tilde{x}_N$ . An effective procedure is suggested by the computation graph: we set

$$\tilde{y}_0 = \tilde{x}_1, \quad \tilde{y}_1 = \tilde{x}_2, \quad \dots, \quad \tilde{y}_{p-1} = \tilde{x}_p \quad (4.8)$$

in the notation of Eq. (3.13) and Eq. (4.4). Assuming the coefficients  $\alpha_i$  and  $\beta_i$  have already been determined, the computation graph shows that knowing the values at stage  $r$  for  $n = 1, 2, \dots, p$  (which is the same as knowing  $y_1, \dots, y_p$  in Eq. (3.13)) allows one to solve for the values at stage  $r-1$  for  $n = 3, 4, \dots, p$ . Iterating, this means we can determine  $z_i^{p-1}, z_i^p$  for all stages  $i$ . From this, it is also straightforward to see that if  $y_0 = \dots = y_{p-1} = 0$ , then  $z_i^{p-1} = z_i^{p-2} = 0$  for  $i = 1, \dots, r$ , so that the initial conditions for Eq. (4.4) are uniquely determined by those of Eq. (3.13).

Once the initial data have been determined and noise generated (as described in Sect. 3), the recurrence relations (4.4) can be iterated to generate predictions from the reduced model.

### 4.3 Fitting models to data

To fit models to data, our strategy is the following:

- (i) From the time series  $\tilde{x}_1, \dots, \tilde{x}_N$ , compute the observations  $\tilde{\Psi}_n = \Psi(\tilde{x}_n)$ .
- (ii) For given parameter vectors  $\alpha, \beta, b$ , use the initial values  $\tilde{x}_1, \dots, \tilde{x}_p$  to determine the initial values  $z_i^{p-2}, z_i^{p-1}, i = 1, \dots, r$ , for Eq. (4.4).
- (iii) Generate one-step predictions  $\hat{x}_{n+1}$  by Eq. (3.15) for  $n = p, \dots, N$ , where  $H(z) = B(z)/A(z)$ .

In the cascade representation, the MSE has the form

$$\mathcal{E}'(\alpha, \beta, b) = \frac{1}{N} \sum_{n=p+1}^N \left\| \tilde{x}_{n+1} - \hat{x}_{n+1}(\tilde{\Psi}_1, \dots, \tilde{\Psi}_n; \alpha, \beta, b) \right\|^2 \quad (4.9)$$

This can be minimized by direct optimization. One then finds the residuals

$$\tilde{\xi}_n = \tilde{x}_{n+1} - \hat{x}_{n+1}(\tilde{\Psi}_1, \dots, \tilde{\Psi}_n; \alpha, \beta, b) \quad (4.10)$$

and fit a noise model as before. One can actually further reduce the dimensionality of the optimization problem; this is described below. But first, we note that Step 3 above is more efficiently implemented by iterating

$$\begin{aligned} \text{Stage 1} \quad z_1^n + \alpha_1 z_1^{n-1} + \beta_1 z_1^{n-2} &= \tilde{\Psi}_{n-p+q} \cdot b_q + \dots + \tilde{\Psi}_{n-p} \cdot b_0 \\ \text{Stage 2} \quad z_2^n + \alpha_2 z_2^{n-1} + \beta_2 z_2^{n-2} &= z_1^n \\ \vdots &\vdots \\ \text{Stage } r \quad z_r^n + \alpha_r z_r^{n-1} + \beta_r z_r^{n-2} &= z_{(r-1)}^n \\ \text{Output} \quad \hat{x}_{n+1} &= z_r^n \end{aligned} \quad (4.11)$$

Modulo transients (see below), this computes the convolutions in Eq. (3.15). Note this iteration can only be carried out if  $\alpha, \beta$  satisfy the decaying memory condition.

To further reduce the dimensionality of the nonlinear optimization problem, first run<sup>2</sup>

$$\begin{aligned} \text{Stage 1} \quad Z_1^n + \alpha_1 Z_1^{n-1} + \beta_1 Z_1^{n-2} &= \Psi_n \\ \text{Stage } i > 1 \quad Z_i^n + \alpha_2 Z_i^{n-1} + \beta_2 Z_i^{n-2} &= Z_{i-1}^n, \end{aligned} \quad (4.12)$$

<sup>2</sup>This algorithm implicitly exploits the commutativity of convolution operators.

for  $i = 2, \dots, r$  and given values of  $(\alpha_1, \beta_1, \dots, \alpha_r, \beta_r)$ , and set  $Y_n = Z_r^n$ . That is, we run the model with  $q = 0$  and  $b_0 = I$ ; note the resulting  $Y_n$  and  $Z_i^n$  are matrix-valued, with the same shape as  $\Psi_n$ . Then, find the minimizers  $(b_0, \dots, b_q)$  of  $\sum_n \|\tilde{x}_{n+1} - y_n\|^2$ , where

$$y_n = Y_{n-p+q} \cdot b_q + \dots + Y_{n-p} \cdot b_0, \quad (4.13)$$

by standard linear regression. Denoting the resulting value of  $b$  by  $\hat{b}(\alpha, \beta)$ , we estimate  $(\alpha, \beta)$  by minimizing

$$\mathcal{E}''(\alpha, \beta) = \frac{1}{N} \sum_n \left\| \tilde{x}_{n+1} - \hat{x}_{n+1}(\tilde{\Psi}_1, \dots, \tilde{\Psi}_n; \alpha, \beta, \hat{b}(\alpha, \beta)) \right\|^2. \quad (4.14)$$

### Remarks.

- (i) *Initial conditions.* In Eq. (4.12), we set  $Z_i^n = 0$  for all stages  $i$  and  $n = 0, \dots, p$ . To account for possible transients due to nonzero initial conditions, we look for initial conditions  $y_h^0, \dots, y_h^p$  so that solutions to the homogeneous recursion  $y_h^n + a_{p-1}y_h^{n-1} + \dots + a_0y_h^{n-p} = 0$  best fit the transient, i.e.,  $Y_{n-p+q} \cdot b_q + \dots + Y_{n-p} \cdot b_0 + y_h^n$  minimizes the mean squared error. This is still a linear regression problem, albeit a larger one.  
(If one instead sets  $y_h^0 = \dots = y_h^p = 0$ , it will not affect the estimated coefficients, but will lead to larger transients in the residuals  $\tilde{\xi}_n$ . This can add a small amount of complexity to inferring a noise model from the residuals.)
- (ii) *Numerical optimization.* Because the optimization problem is now nonlinear in  $(\alpha, \beta)$ , and because the factorized form introduces a permutation symmetry into the cost function, the optimization problem is now highly non-convex: there are many equivalent global minima, which introduce many saddles into the landscape and can potentially slow down optimizers. It may be possible to avoid this problem using other representations than (4.4). We opted for Eq. (4.4) in this paper for its simplicity; other representations will be studied in the future.

Also, we have opted for direct nonlinear minimization of  $\mathcal{E}''(\alpha, \beta)$  in this paper. It may be possible to improve the efficiency of the optimization by exploiting the structure of Eq. (4.4) or the multistep representation (Eq. (3.14) above) by using, e.g., iterative least squares.

**Source code.** We have implemented the algorithms described above as a general package in Julia version 1.1 ([42]). For numerical optimization, we used the NLOpt.jl package ([43]). The source code is being prepared for public release; interested readers should contact the authors.

## 5 Examples

### 5.1 Kuramoto-Sivashinsky (KS) PDE

The KS equation

$$U_t + UU_x + U_{xx} + U_{xxxx} = 0 \quad (5.1)$$

is a prototypical model of spatiotemporal chaos. Here, we consider Eq. (5.1) with  $0 \leq x \leq L$  and periodic boundary conditions. In Fourier variables  $u_k(t)$ , Eq. (5.1) is

$$\dot{u}_k = -\frac{i\lambda_k}{2} \sum_{\ell} u_{\ell} u_{k-\ell} + (\lambda_k^2 - \lambda_k^4)u_k, \quad \lambda_k = \frac{2\pi k}{L}. \quad (5.2)$$

The lowest  $\approx L/2\pi$  modes are linearly unstable. This long-wave instability and its interaction with the quadratic nonlinearity lead to sustained chaotic behavior, with positive Lyapunov exponents and exponential decay of correlations [44]. NARMAX modeling of Eq. (5.1) was studied in [36], using likelihood-based parameter estimation and a slightly different form of NARMAX. Here, we use the least squares procedure. Following [36], we set  $L \approx 21.55$ , leading to 3 linearly unstable modes and a maximum Lyapunov exponent of  $\approx 0.04$  (Lyapunov time  $\approx 25$ ). In this regime, time correlation functions exhibit complex oscillations instead of the simple exponential decay often seen in strongly chaotic systems (Fig. 2(a)), providing a nontrivial testbed for model reduction.

Eq. (5.1) is readily solved by truncating the Fourier series, provided the cutoff is large enough. Here, we take as full model the 96-mode truncation; numerical tests show that KS statistics are insensitive to the cutoff beyond this. Fig. 1(a) shows a sample solution of Eq. (5.1) using this 96-mode truncation (“full”). By comparison, the

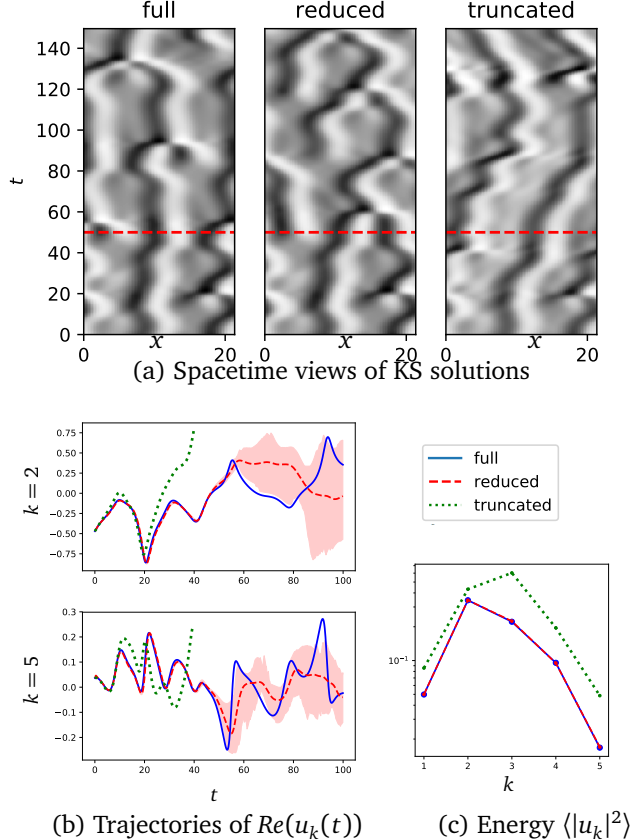


Figure 1: KS solutions. Panel (a) shows results computed using the 96-mode truncation ( $\Delta t = 10^{-3}$ ) (left), the 5-mode reduced model ( $\Delta t = 0.1$ ) (middle), and the 5-mode truncation ( $\Delta t = 10^{-3}$ ) (right). In (b), we plot two Fourier modes as functions of time, with 90% confidence intervals for the reduced model. Panel (c) shows the energy spectrum.

5-mode truncation with the same initial conditions (“truncated”) diverges rapidly, and fails to reproduce the energy spectrum (Fig. 1(c)).

*Reduced model.* To construct a reduced model using the lowest  $K = 5$  Fourier modes, we follow the procedure outlined in Sect. 3. The first step is to generate data from the full model, which we do by numerically integrating the 96-mode truncation using a 4th-order exponential time-differencing Runge-Kutta (ETDRK4) method [45, 46] with timestep  $\Delta t = 10^{-3}$ , for  $10^8$  steps. We observe the first  $K = 5$  Fourier modes at every 100 steps; the observation interval  $\delta = 0.1$  is the timestep for the reduced model. We drop the first half of the data to ensure stationarity.

We use the form of the reduced model in Eq. (3.13). For the function  $\Psi(u)$ , we use two groups of basis functions. The first group is defined by  $\varphi_k(u)$ ,  $k = 1 \cdots 5$ , consists of numerical predictions based on the 5-mode truncation. More precisely, we take the nonlinear part of Eq. (5.2), i.e., a 5-mode truncation of the inviscid Burgers equation, and integrate it numerically by one step  $\Delta t$  to produce a rough estimate  $\varphi_k(u)$  of the  $k$ th Fourier mode using the lowest 5 modes  $u = (u_1, \dots, u_5)$  from the previous step. Since the 5-mode truncation is much less stiff than the 96-mode model, we use a standard RK4 method for this. The second group consists of additional nonlinearities  $\theta_k(u)$  motivated by the theory of approximate inertial manifolds [47] (see A and [36]). The observation function  $\Psi(u)$  is the  $5 \times 10$  matrix given by  $[\varphi_1(u)e_1, \dots, \varphi_5(u)e_5, \theta_1(u)e_1, \dots, \theta_5(u)e_5]$ ,  $e_k$  being the  $k$ th Euclidean basis vector; this form of  $\Psi(u)$  essentially fits a separate linear filter to each mode. Terms linear in  $x$  are omitted because they can be accounted for by the coefficients  $b_i$  (as suggested by exponential integrator formulas [45, 46]), and linear terms can lead to degeneracy in Eq. (3.14) (equivalently Eq. (3.13)): different parameters can yield the same model.

Finally, the reduced model is fit to data by the procedure outlined in Sect. 3. As was found in [36], not all combinations of  $p$  and  $q$  lead to stable reduced models. Indeed, we have experimented with “replaying” the residuals, i.e., compute the residuals  $\tilde{\xi}_n$  as in Sect. 5, then running the reduced model with  $\tilde{\xi}_{n+1}$  in place of the

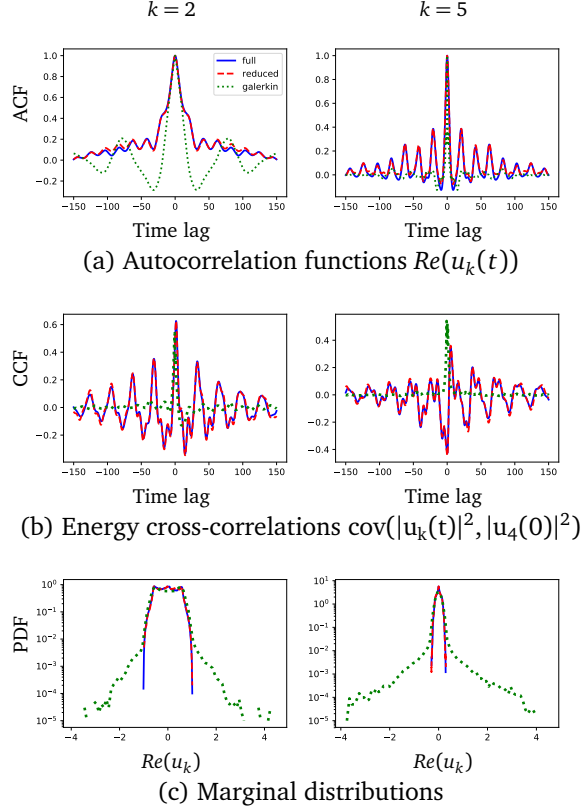


Figure 2: KS statistics. In all panels, solid blue is the full model, dashed red is the reduced model, and dotted green is the 5-mode truncation. Panel (a) shows autocorrelation functions for two Fourier modes  $Re(u_k(t))$ . In (b), we show cross correlation functions for the energies  $|u_k(t)|^2$  and  $|u_4(0)|^2$  for  $k = 2, 5$ . In (c), distributions of  $Re(u_k)$  are shown.

noise term. In the absence of round-off, one would simply obtain  $x_n = \tilde{x}_n$ , i.e., reconstruct the original time series. Instead, for some choices of  $(p, q)$ , round-off errors were rapidly amplified. Here, we use  $p = q = 2$ . As measured by the product of the mode and step counts, the reduced model represents a near 400-fold reduction in computational cost.

*Results.* Fig. 1(a) compares the full model (“full”), the reduced model with  $p = q = 2$  (“reduced”), and the 5-mode truncation with  $\Delta t = 10^{-3}$  (“truncated”). As one can see, the reduced model reproduces the full solution up to  $t \gtrsim 50$ , about  $1.8 \times$  the Lyapunov time, consistent with [36]. In contrast, the 5-mode truncation is accurate for a fraction of that time. Fig. 1(b) takes a closer look at selected Fourier modes. For the reduced model, 100 independent realizations are run, and the resulting ensemble is used to estimate confidence intervals. Shown is the mean (dashed, red), and 90% confidence intervals. Though the noise terms have amplitudes  $\leq 10^{-4}$ , they are rapidly amplified by exponential separation of trajectories due to the long-wave instability in KS. Consistent with Fig. 1(a), the mean follows the true trajectory up to  $t \approx 40$ , at which point they begin to diverge. In contrast, the 5-mode truncation diverges by  $t \approx 20$ . Moreover, even when the confidence interval starts to widen, it continues to provide useful bounds for some time. Eventually the ensemble approaches statistical steady state, and the ensemble mean converges toward its expected value. Fig. 1(c) compares the energy spectra  $\langle |u_k|^2 \rangle$ : while the reduced model correctly predicts the spectrum, the 5-mode truncation produces fluctuations that are too large.

In Fig. 2, we examine long-time statistics. In (a), we compare the autocorrelation functions (ACFs) of selected Fourier modes. Unlike the 5-mode truncation, the reduced model is able to reproduce quite complex features in the ACFs. Fig. 2(b) shows cross correlation functions for the energy of the  $k$ th mode with the energy of the 4th mode, i.e.,  $\text{cov}(|u_k^n|^2, |u_4^0|^2)$  as a function of the time lag  $n\Delta t$ ; such cross correlation functions (CCF) can be viewed as a measure of energy transfer between modes. The reduced model correctly predicts these 4th moments, showing that the reduced model captures genuinely nonlinear effects in KS dynamics. Panel (c) shows the reduced model is able to reproduce marginal distributions, whereas the 5-mode truncation produces marginals that are too

wide (compare with Fig. 1(c)). We conclude that both in terms of short-time forecasting and long-time statistics, the reduced model effectively captures KS dynamics. These findings are consistent with [36], suggesting the likelihood-based estimator used in [8, 36] and the least squares estimator above are comparable, and the NARMAX model in [36] nearly optimal in the least squares sense.

## 5.2 Stochastically-forced Burgers equation

Now consider a stochastically-forced viscous Burgers equation

$$U_t + UU_x = \nu U_{xx} + \eta \quad (5.3)$$

with  $\eta(t, x)$  white in  $t$  and smooth in  $x$ , and  $U(t, x)$   $2\pi$ -periodic in  $x$ . More precisely, in Fourier variables,

$$\dot{u}_k = -\frac{i\lambda_k}{2} \sum_{\ell} u_{\ell} u_{k-\ell} - \nu \lambda_k^2 u_k + \sigma_k \dot{w}_k, \quad (5.4)$$

where  $\sigma_k = 1$  for  $|k| \leq 4$  and  $\sigma_k = 0$  for  $|k| > 4$ , and  $\dot{w}_k$  is white noise. In contrast to the KS equation, which is deterministic and exhibits self-sustained chaos, the viscous Burgers equation is dissipative: without forcing, all solutions converge to the steady state  $u \equiv 0$  as  $t \rightarrow \infty$ . Stationary statistics of  $u(x, t)$  thus reflect a balance between the forcing  $\eta$  and dissipation through viscosity. We note that the stochastic Burgers equation has the so-called “one force one solution” (1F1S) property [48]: for a given realization of  $\eta_t, t \geq 0$ , all initial conditions lead asymptotically to the same (time dependent) solution. Put another way, modulo transients, solutions of Eq. (5.4) are determined by the forcing.

In view of the 1F1S property, a natural question is: given a specific realization of the forcing  $\eta_t$ , can a reduced model correctly predict the response of the system? To test this, we compare a fully-resolved, 128-mode truncation of Eq. (5.4) with an under-resolved 9-mode truncation and a 9-mode reduced model inferred from data. Throughout,  $\nu = 0.05$ . (See [49] for an alternate view of this problem.)

*Data-driven reduced model.* To generate data from the full model, we solve Eq. (5.4) using a scheme of the form

$$u_k^{n+1} = G_k(u^n, \Delta t) + \sqrt{\Delta t} \sigma_k \eta_k^n, \quad (5.5)$$

where  $G_k(u, \Delta t)$  is the result of applying ETDRK4 to the deterministic part of Eq. (5.4),  $u_k^n = u_k(n\Delta t)$ ,  $u^n = (u_1^n, \dots, u_K^n)$ , and  $\eta_k^n$  independent  $N(0, 1)$  random variables. Like the standard Euler-Maruyama scheme, Eq. (5.5) has weak order 1, but is more stable [50]. We solve the full system with timestep  $\Delta t = 0.00125$  and observe every 8th step, so the reduced model has timestep  $\delta = 0.01$ .

To account for the forcing, we modify Eq. (3.13) to obtain

$$x_{n+1} = y_n + \xi_{n+1}, \quad (5.6a)$$

$$y_n + a_{p-1} y_{n-1} + \dots + a_0 y_{n-p} \quad (5.6b)$$

$$= \Psi_{n-p+q} \cdot b_q + \dots + \Psi_{n-p} \cdot b_0 + \quad (5.6c)$$

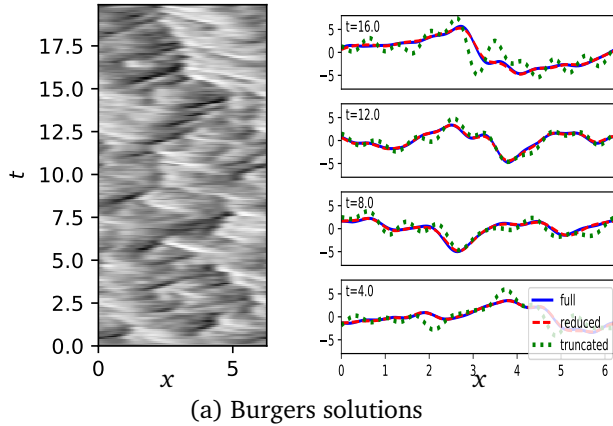
$$c_q \bar{\eta}_{n+q} + \dots + c_0 \bar{\eta}_n. \quad (5.6d)$$

The  $\bar{\eta}_n$  in the moving average (5.6d) are related to the forcing  $\eta^n$  in Eq. (5.5) by  $\bar{\eta}^n = (\eta^{8n} + \dots + \eta^{8n+7})/\sqrt{8}$ ; this correlates the full model and the reduced model during fitting. The independent noise term  $\xi_n$  is inferred from the residuals as before, and permits one to quantify the uncertainty in response prediction via ensemble forecasting. As noted in Sect. 3.5, random dynamical systems like Eq. (5.4) are encompassed within MZ theory, and Eq. (5.6) can be seen as a special case of the Wiener projection

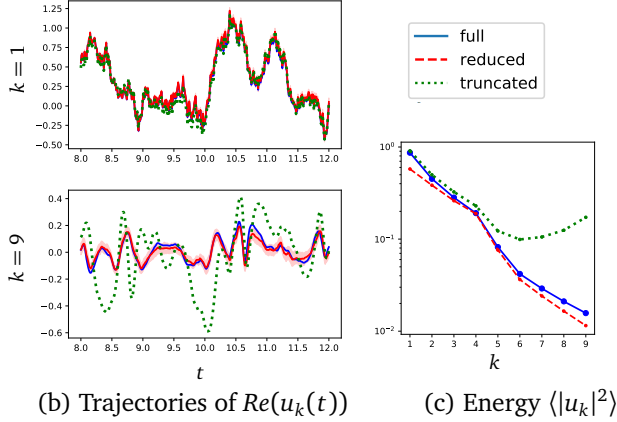
We have also constructed reduced models of the form (3.13), which do not correlate the reduced and full models through shared forcing. All else being equal, we found the performance of Eq. (5.6) to be strictly better in our tests than Eq. (3.13) because more information is retained. We report results obtained using Eq. (5.6) with  $p = q = 1$ , leading to a  $\sim 50$ -fold reduction in cost.

*Results.* Fig. 3(a) shows sample solutions. The 1F1S property suggests that the low modes in the full, reduced, and the 9-mode truncation models will all be strongly correlated, as confirmed in the snapshots. However, one also sees that the 9-mode truncation exhibits significant deviations from the full model, unlike the reduced model. Panels (b) and (c) shows this behavior in more details: because of the forcing, the low modes of all 3 models stay close over time, but the 9-mode truncation shows relatively large deviations from the full model. As before, Fig. 3(b) shows 90% confidence intervals for the reduced model, computed using an ensemble of 100 trajectories.

Spacetime view, full model Snapshots (legend below)



(a) Burgers solutions



(b) Trajectories of  $Re(u_k(t))$

(c) Energy  $\langle |u_k|^2 \rangle$

Figure 3: Stochastic Burgers solutions. Panel (a) shows results computed using the 128-mode truncation with  $\Delta t = 0.00125$  (left), and snapshots of the full model, the 9-mode reduced model ( $\Delta t = 0.01$ ), and the 9-mode truncation ( $\Delta t = 0.00125$ ). In (b), we plot two Fourier modes as functions of time, with 90% confidence intervals for the reduced model. Panel (c) shows the energy spectrum.

As expected, the forced modes are tightly entrained to each other, whereas the 9-mode truncation shows significant deviation in higher modes. Because of the 1F1S property, the reduced model can be expected to correctly forecast the response for as long as information about the forcing is available. As for the KS equation, the reduced model here also reproduces long-time statistics; see Fig. 3(c) for the energy spectrum and B for other statistics.

Finally, we note that while accurate response forecasting will clearly become more difficult for larger observation intervals, the reduced model can nevertheless capture long-time statistics for much larger observation times. Indeed, we have tested the reduced model for much larger observation intervals, up to 0.1 (see B).

## 6 Concluding discussion

We have shown that by combining ideas from MZ and Wiener filtering, the Wiener projection provides a starting point for systematic data-driven model reduction. Within this framework, we derive the NARMAX model widely used in time series modeling and analysis, providing an interpretation of NARMAX in terms of an underlying dynamical system and evidence that it may be nearly optimal in the sense of least squares. The Wiener projection view of NARMAX also clarifies the scope of NARMAX-like approaches and their relation to the Mori-Zwanzig formalism. Using the KS and stochastic Burgers equations, we have demonstrated the flexibility and effectiveness of this view of model reduction for chaotic and random dynamics.

Wiener projection may serve as the starting point for approximations beyond NARMAX. For example, while we have focused on parametric reduction here, in principle the observation functions can be inferred from data using nonparametric methods like delay coordinates, manifold learning, dynamic model decomposition, reservoir

computing, and other machine learning techniques [51, 52, 53, 54, 55, 56, 57]. The Wiener projection formulation complements and extends existing strategies for data-driven modeling and model reduction by providing a systematic guide to incorporating memory and noise effects, in situations without sharp scale separation.

**Acknowledgments.** We thank the Mathematics Group at Lawrence Berkeley National Lab for its support of this work; to Alexandre Chorin for many useful comments on the manuscript; and to Xiantao Li for encouraging us to study the discrete Mori-Zwanzig formalism. KL was supported by NSF grant DMS-1821286, and FL was supported by NSF grant DMS-1821211.

## References

- [1] G. Pavliotis, A. Stuart, *Multiscale methods: averaging and homogenization*, Springer Science & Business Media, 2008.
- [2] I. G. Kevrekidis, G. Samaey, *Equation-free multiscale computation: Algorithms and applications*, *Annu. Rev. Phys. Chem.* 60 (2009).
- [3] A. J. Roberts, *Model emergent dynamics in complex systems*, Vol. 20, SIAM, 2014.
- [4] A. Abdulle, E. Weinan, B. Engquist, E. Vanden-Eijnden, *The heterogeneous multiscale method*, *Acta Numerica* 21 (2012) 1–87.
- [5] A. J. Chorin, O. H. Hald, *Stochastic Tools in Mathematics and Science*, Springer, 2013.
- [6] R. Zwanzig, *Nonequilibrium Statistical Mechanics*, Oxford, 2001.
- [7] D. Kondrashov, M. D. Chekroun, M. Ghil, *Data-driven non-Markovian closure models*, *Physica D* 297 (2015) 33–55. doi:10.1016/j.physd.2014.12.005.
- [8] A. J. Chorin, F. Lu, *Discrete approach to stochastic parametrization and dimension reduction in nonlinear dynamics*, *Proc. Natl. Acad. Sci. USA* 112 (32) (2015) 9804–9809.
- [9] J. Harlim, X. Li, *Parametric reduced models for the nonlinear Schrödinger equation*, *Physical Review E* 91 (5) (2015). doi:10.1103/PhysRevE.91.053306.
- [10] H. Lei, N. A. Baker, X. Li, *Data-driven parameterization of the generalized Langevin equation*, *Proc. Natl. Acad. Sci. USA* 113 (50) (2016) 14183–14188. doi:10.1073/pnas.1609587113.
- [11] X. Xie, M. Mohebujjaman, L. G. Rebholz, T. Iliescu, *Data-Driven Filtered Reduced Order Modeling of Fluid Flows*, *SIAM J. Sci. Comput.* 40 (3) (2018) B834–B857. doi:10.1137/17M1145136.
- [12] M. D. Chekroun, D. Kondrashov, *Data-adaptive harmonic spectra and multilayer Stuart-Landau models*, *Chaos: An Interdisciplinary Journal of Nonlinear Science* 27 (9) (2017) 093110. arXiv:1706.04275, doi:10.1063/1.4989400.
- [13] J. D. Hamilton, *Time Series Analysis*, Princeton University Press, Princeton, NJ, 1994.
- [14] S. A. Billings, *Nonlinear System Identification: NARMAX Methods in the Time, Frequency, and Spatiotemporal Domains*, John Wiley and Sons, 2013.
- [15] F. Lu, K. K. Lin, A. J. Chorin, *Comparison of continuous and discrete-time data-based modeling for hypoelliptic systems*, *Comm. App. Math. Com. Sc.* 11 (2) (2016) 187–216.
- [16] A. J. Chorin, O. H. Hald, *Stochastic Tools in Mathematics and Science*, 3rd Edition, Springer, New York, NY, 2013.
- [17] A. J. Chorin, O. H. Hald, R. Kupferman, *Optimal prediction with memory*, *Physica D: Nonlinear Phenomena* 166 (3-4) (2002) 239–257.
- [18] L. Ma, X. Li, C. Liu, *Coarse-graining Langevin dynamics using reduced-order techniques*, *J. Comput. Phys.* 380 (2019) 170–190. doi:10.1016/j.jcp.2018.11.035.

[19] H. Cho, D. Venturi, G. E. Karniadakis, Statistical analysis and simulation of random shocks in stochastic burgers equation, *Proceedings of the Royal Society A: Mathematical, Physical and Engineering Sciences* 470 (2171) (2014) 20140080.

[20] Z. Li, H. S. Lee, E. Darve, G. E. Karniadakis, Computing the non-markovian coarse-grained interactions derived from the mori-zwanzig formalism in molecular systems: Application to polymer melts, *J. Chem. Phys.* 146 (1) (2017) 014104.

[21] Z. Li, X. Bian, X. Li, G. E. Karniadakis, Incorporation of memory effects in coarse-grained modeling via the mori-zwanzig formalism, *The Journal of chemical physics* 143 (24) (2015) 243128.

[22] A. Panchenko, L. L. Barannyk, R. P. Gilbert, Closure method for spatially averaged dynamics of particle chains, *Nonlinear Analysis: Real World Applications* 12 (3) (2011) 1681–1697. doi:10.1016/j.nonrwa.2010.10.021.  
URL <http://www.sciencedirect.com/science/article/pii/S1468121810002968>

[23] S. C. Venkataramani, R. C. Venkataramani, J. M. Restrepo, Dimension reduction for systems with slow relaxation, *Journal of Statistical Physics* 167 (3-4) (2017) 892–933.

[24] P. Stinis, Stochastic optimal prediction for the Kuramoto–Sivashinsky equation, *Multiscale Modeling & Simulation* 2 (4) (2004) 580–612.

[25] E. J. Parish, K. Duraisamy, Non-markovian closure models for large eddy simulations using the mori-zwanzig formalism, *Physical Review Fluids* 2 (1) (2017) 014604.

[26] S. Wang, Z. Li, W. Pan, Implicit-solvent coarse-grained modeling for polymer solutions via Mori-Zwanzig formalism, *Soft Matter* (2019). doi:10.1039/C9SM01211G.  
URL <http://dx.doi.org/10.1039/C9SM01211G>

[27] E. Darve, J. Solomon, A. Kia, Computing generalized Langevin equations and generalized Fokker-Planck equations, *Proc. Natl. Acad. Sci. USA* 106 (2009) 10884–10889.

[28] H. Grabert, *Projection Operator Techniques in Nonequilibrium Statistical Mechanics*, Springer, 1982.

[29] D. Forster, *Hydrodynamic fluctuations, broken symmetry, and correlation functions*, CRC Press, 2018.

[30] J. Fan, Q. Yao, *Nonlinear Time Series: Nonparametric and Parametric Methods*, Springer, New York, NY, 2003.

[31] E. J. Hannan, *Multiple Time Series*, John Wiley and Sons, 1970.

[32] T. Kailath, *Lectures on Wiener and Kalman Filtering*, Springer, 1981.

[33] M. Brin, G. Stuck, *Introduction to dynamical systems*, Cambridge university press, 2002.

[34] W. H. Press, S. A. Teukolsky, W. T. Vetterling, B. P. Flannery, *Numerical recipes 3rd edition: The art of scientific computing*, Cambridge university press, 2007.

[35] C. Cameron, Relative efficiency of gaussian stochastic process sampling procedures, *J. Comput. Phys.* 192 (2) (2003) 546–569.

[36] F. Lu, K. K. Lin, A. J. Chorin, Data-based stochastic model reduction for the Kuramoto–Sivashinsky equation, *Physica D* 340 (2017) 46–57.

[37] F. Ledrappier, L. S. Young, Entropy formula for random transformations, *Probability theory and related fields* 80 (2) (1988) 217–240.

[38] Y. Kifer, *Ergodic theory of random transformations*, Vol. 10, Springer Science & Business Media, 2012.

[39] L. Arnold, *Random dynamical systems*, Springer Science & Business Media, 2013.

[40] P. H. Baxendale, The lyapunov spectrum of a stochastic flow of diffeomorphisms, in: *Lyapunov Exponents*, Springer, 1986, pp. 322–337.

[41] H. Kunita, *Stochastic flows and stochastic differential equations*, Vol. 24, Cambridge university press, 1997.

[42] J. Bezanson, A. Edelman, S. Karpinski, V. B. Shah, Julia: a fresh approach to numerical computing, *SIAM Review* 59 (2017) 65–98.

[43] S. G. Johnson, The NLOpt nonlinear-optimization package (2019).  
URL <http://ab-initio.mit.edu/nlopt>

[44] J. M. Hyman, B. Nicolaenko, The Kuramoto-Sivashinsky equation: a bridge between PDEs and dynamical systems, *Physica D* 18 (1986) 113–126.

[45] S. M. Cox, P. C. Matthews, Exponential time differencing for stiff systems, *J. Comput. Phys.* 176 (2) (2002) 430–455.

[46] A. K. Kassam, L. N. Trefethen, Fourth-order time stepping for stiff PDEs, *SIAM J. Sci. Comput.* 26 (4) (2005) 1214–1233.

[47] M. S. Jolly, I. G. Kevrekidis, E. S. Titi, Approximate inertial manifolds for the Kuramoto-Sivashinsky equation: analysis and computations, *Physica D* 44 (1) (1990) 38–60.

[48] W. E, K. Khanin, A. Mazel, Y. Sinai, Invariant measure for Burgers equation with stochastic forcing, *Ann. Math.* 151 (3) (2000) 877–960.

[49] J. Bunder, A. J. Roberts, Resolution of subgrid microscale interactions enhances the discretisation of nonautonomous partial differential equations, *Applied Mathematics and Computation* 304 (2017) 164–179.

[50] P. E. Kloeden, E. Platen, *Numerical Solution of Stochastic Differential Equations*, 3rd Edition, Springer, Berlin, 1999.

[51] B. A. Freno, K. T. Carlberg, Machine-learning error models for approximate solutions to parameterized systems of nonlinear equations, *Computer Methods in Applied Mechanics and Engineering* 348 (2019) 250–296.

[52] S. L. Brunton, J. L. Proctor, J. N. Kutz, Discovering governing equations from data by sparse identification of nonlinear dynamical systems, *Proc. Natl. Acad. Sci. USA* (2016) 201517384.

[53] S. W. Jiang, J. Harlim, Modeling of Missing Dynamical Systems: Deriving Parametric Models using a Nonparametric Framework, *arXiv:1905.08082* (May 2019).  
URL <http://arxiv.org/abs/1905.08082>

[54] D. Mukhin, A. Gavrilov, A. Feigin, E. Loskutov, J. Kurths, Principal nonlinear dynamical modes of climate variability, *Scientific Reports* 5 (2015) 15510. doi:10.1038/srep15510.  
URL <http://www.nature.com/srep/2015/151022/srep15510/full/srep15510.html>

[55] T. Berry, J. R. Cressman, Z. Gregurić-Ferenček, T. Sauer, Time-Scale Separation from Diffusion-Mapped Delay Coordinates, *SIAM J Appl. Dyn. Syst.* 12 (2) (2013) 618–649. doi:10.1137/12088183X.  
URL <http://pubs.siam.org/doi/abs/10.1137/12088183X>

[56] C. Ma, J. Wang, W. E, Model reduction with memory and the machine learning of dynamical systems, *arXiv:1808.04258* (2018).

[57] J. Pathak, B. Hunt, M. Girvan, Z. Lu, E. Ott, Model-Free Prediction of Large Spatiotemporally Chaotic Systems from Data: A Reservoir Computing Approach, *Phys. Rev. Lett.* 120 (2) (2018). doi:10.1103/PhysRevLett.120.024102.

[58] D. Crommelin, E. Vanden-Eijnden, Subgrid-scale parameterization with conditional Markov chains, *J. Atmos. Sci* 65 (8) (2008) 2661–2675.

## A Kuramoto-Sivashinsky equation

### Nonlinear terms in the NARMAX model

The Kuramoto-Sivashinsky example in Sect. 5 uses the reduced model from [36]. For the convenience of readers, the full *ansatz* is reproduced here:

$$u_k^{n+1} = u_k^n + R_k^{\Delta t}(u^n) \Delta t + z_k^n \Delta t, \quad (\text{A.1a})$$

$$z_k^{n+1} = \Phi_k^n + \xi_k^{n+1}, \quad (\text{A.1b})$$

$$\begin{aligned} \Phi_k^n = & \sum_{j=0}^p a_{k,j} z_k^{n-j} + \sum_{j=0}^r b_{k,j} u_k^{n-j} + c_{k,(K+1)} R_k^{\Delta t}(u^n) \\ & + i \sum_{j=1}^K c_{k,j} \tilde{u}_{j+K}^n \overline{\tilde{u}_{j+K-k}^n} + \sum_{j=0}^q d_{k,j} \xi_k^{n-j}, \end{aligned} \quad (\text{A.1c})$$

where

$$\tilde{u}_j^n = \begin{cases} u_j^n, & 1 \leq j \leq K \\ i \sum_{\ell=j-K}^K u_{\ell}^n u_{j-\ell}^n, & K < j \leq 2K. \end{cases} \quad (\text{A.1d})$$

The nonlinear terms in Eqs. (A.1c) and (A.1d) are suggested by inertial manifold theory. See [36] for details.

We compare the *ansatz* to a model of the form (4.4) with predictors

$$\psi_1(u) = u, \quad (\text{A.2a})$$

$$\psi_2(u) = R^{\Delta t}(u), \quad (\text{A.2b})$$

$$\psi_j(u) = \tilde{u}_{j+K} \overline{\tilde{u}_{j+K-k}}, \quad j = 1, \dots, K. \quad (\text{A.2c})$$

It is straightforward to show that the *ansatz* in Eq. (A.1) is equivalent to a model of the form

$$x_{n+p'+1} + a_{p'-1} x_{n+p'} + \dots + a_0 x_{n+1} = \Psi_{n+q'} \cdot b_{q'} + \dots + \Psi_n \cdot b_0 + \xi'_{n+1}, \quad (\text{A.3})$$

for some choice of orders  $p', q'$ , coefficients  $a_i, b_i$ , and noise  $\xi'_{n+1}$ . (This is Eq. (3.14).)

In addition to the use of a least-squares estimator, the reduced model in Eq. (A.2) differs from the reduced model in Eq. (A.1) in that

- (i) Eq. (A.2) models the noise by a Gaussian process using power spectrum from the residual  $\tilde{\xi}_n$ , whereas Eq. (A.1) models the noise by a moving average process.
- (ii) as suggested by the Wiener projection formalism, Eq. (A.2) contains time-delayed copies of all nonlinear terms, whereas Eq. (A.1) does not.

### Detailed Numerical results

Figs. 4 and 5 are full versions of the numerical results shown in Sect. 5.1.

To further quantify finite-time forecasts as a function of the “lead time” (i.e., time since initial observation), we introduce two standard measures of forecasting “skill,” the root mean squared error and the anomaly correlation. Both are based on ensemble forecasts in the following way: let  $v(t_n)$  denote the time series data for the full model, and take  $N_0$  short pieces, i.e.,  $\{(v(t_n), n = n_i, n_i + 1, \dots, n_i + T)\}_{i=1}^{N_0}$  with  $n_{i+1} = n_i + T_{\text{lag}}/\Delta t$ , where  $T = T_{\text{lag}}/\Delta t$  is the length of each piece and  $T_{\text{lag}}$  is the time gap between two adjacent pieces. For each short piece  $(v(t_n), n = n_i, \dots, n_i + T)$ , we generate  $N_{\text{ens}}$  trajectories of length  $T$  from the reduced model, starting all ensemble members from the same initial segment  $(v(t_{n_i}), v(t_{n_i+1}), \dots, v(t_{n_i+m}))$ , where  $m = 2p + 1$ , and denote the sample trajectories by  $(u^n(i, j), n = 1, \dots, T)$  for  $i = 1, \dots, N_0$  and  $j = 1, \dots, N_{\text{ens}}$ .

Again, we do not introduce artificial perturbations into the initial conditions, because the exact initial conditions are known, and by initializing from data, we preserve the memory of the system so as to generate better ensemble trajectories.

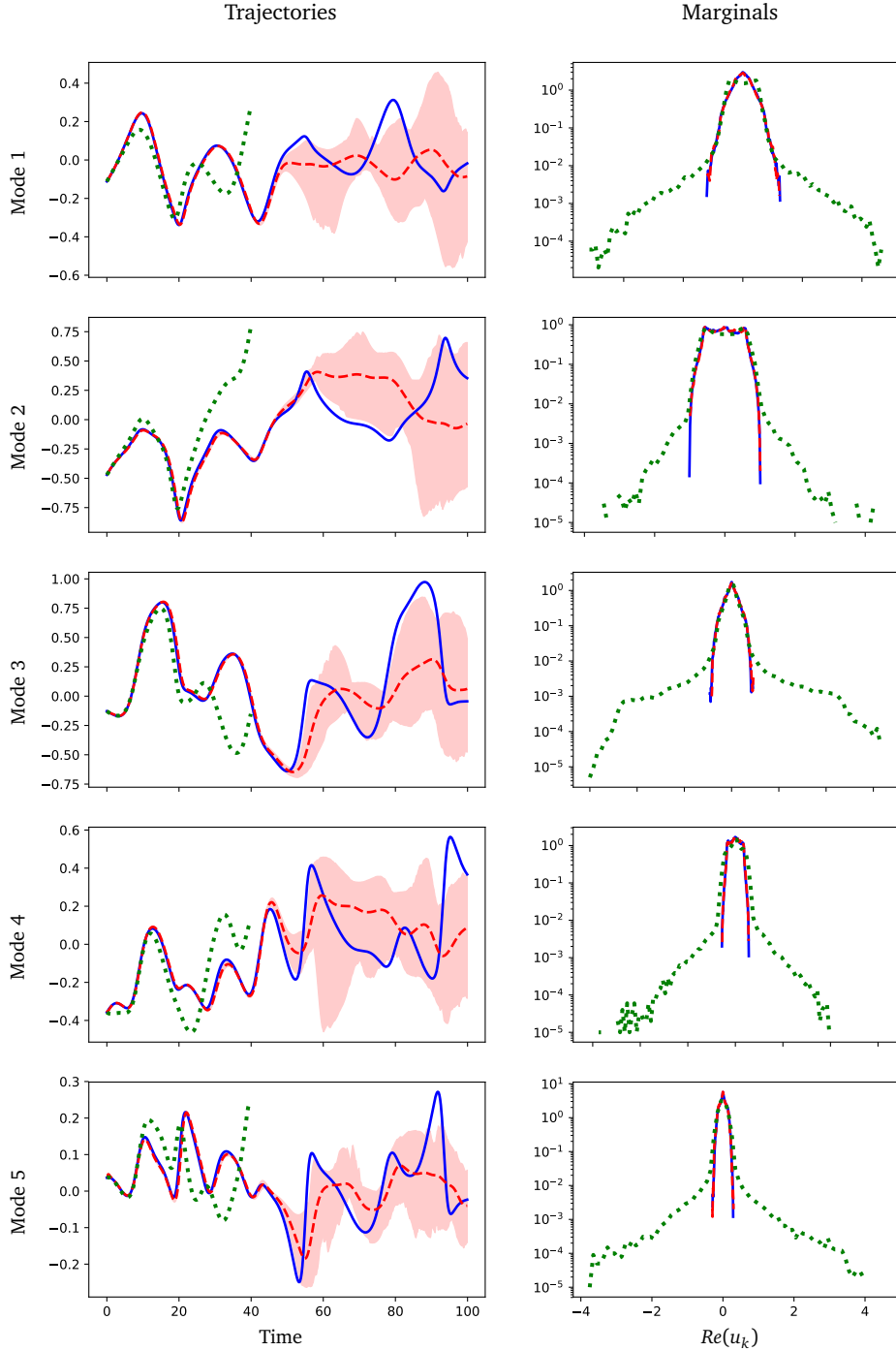


Figure 4: Comparison of finite-time forecasts and marginal distributions. In all panels, solid blue line is the full model (96-mode truncation), dashed red line is the 5-mode reduced model, and dotted green line the 5-mode truncation. *Left:* trajectories starting from the same initial conditions. For the reduced model, we show the 5th percentile, mean, and 95th percentile, computed with an ensemble of size 100. The truncated model was terminated at  $t = 40$  to reduce clutter. *Right:* marginal densities.

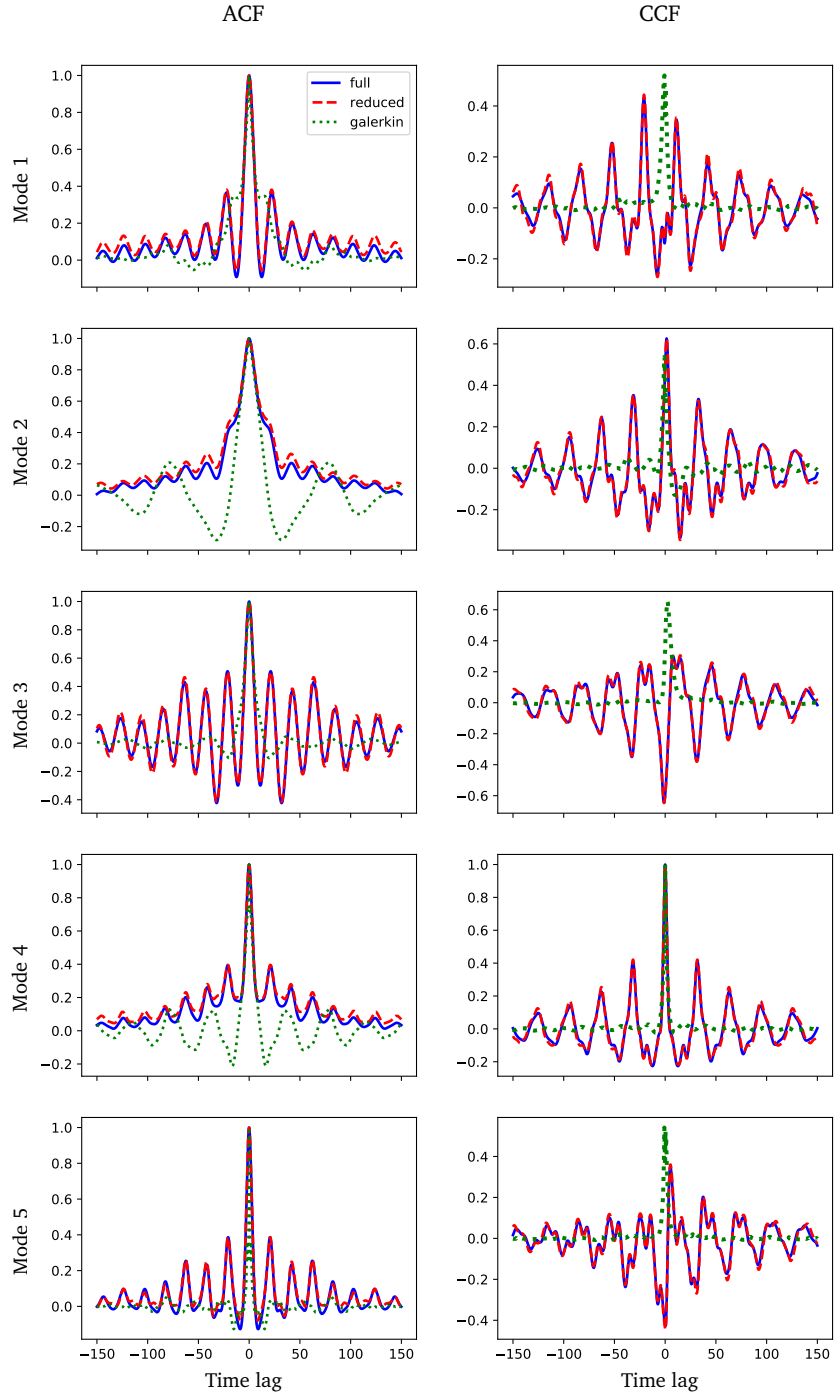


Figure 5: Comparison of autocorrelation functions (ACFs) and energy cross correlation functions (CCFs). In all panels, solid blue line is the full model (96-mode truncation), dashed red line is the 5-mode reduced model, and dotted green line the 5-mode truncation. *Left:* Autocorrelation functions for  $\text{Re}(u_k(t))$  for  $k = 1, \dots, 5$ . *Right:* Cross correlations between  $|u_4(t)|^2$  and  $|u_k(t)|^2$  for  $k = 1, \dots, 5$ .

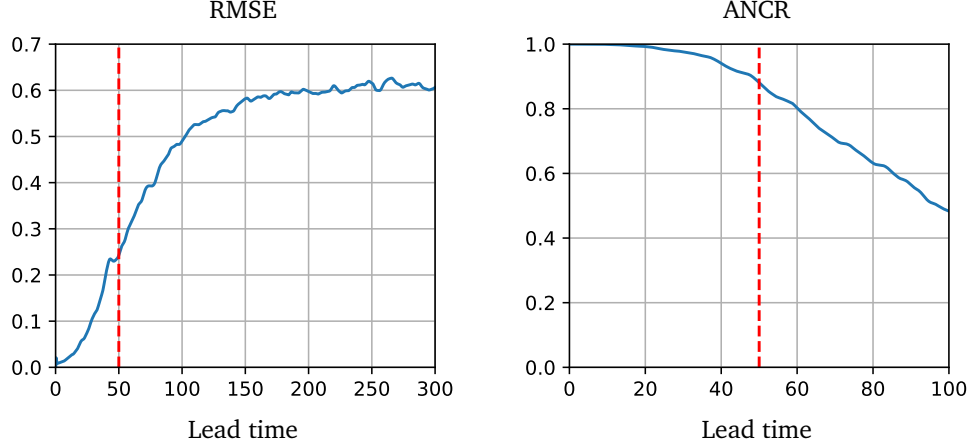


Figure 6: Forecasting skill as function of lead time of the reduced model for the KS equation. *Left:* root mean squared error (RMSE). *Right:* anomaly correlation (ANCR). See text for details.

The *root mean squared error* is

$$\text{RMSE}(\tau_n) := \left( \frac{1}{N_0} \sum_{i=1}^{N_0} |\text{Re } v(t_{n_i+n}) - \text{Re } \bar{u}^n(i)|^2 \right)^{1/2}, \quad (\text{A.4})$$

where  $\tau_n = n\Delta t$ ,  $\bar{u}^n(i) = \frac{1}{N_{\text{ens}}} \sum_{j=1}^{N_{\text{ens}}} u^n(i, j)$ , and the *anomaly correlation* (see, e.g., [58]) is

$$\text{ANCR}(\tau_n) := \frac{1}{N_0} \sum_{i=1}^{N_0} \frac{\mathbf{a}^{v,i}(n) \cdot \mathbf{a}^{u,i}(n)}{\sqrt{|\mathbf{a}^{v,i}(n)|^2 |\mathbf{a}^{u,i}(n)|^2}}, \quad (\text{A.5})$$

where  $\mathbf{a}^{v,i}(n) = \text{Re } v(t_{n_i+n}) - \text{Re } \langle v \rangle$  and  $\mathbf{a}^{u,i}(n) = \text{Re } \bar{u}^n(i) - \text{Re } \langle v \rangle$  are the anomalies in data and the ensemble mean. Here  $\mathbf{a} \cdot \mathbf{b} = \sum_{k=1}^K a_k b_k$ ,  $|\mathbf{a}|^2 = \mathbf{a} \cdot \mathbf{a}$ , and  $\langle v \rangle$  is the time average of the long trajectory of  $v$ . Both statistics measure the accuracy of the mean ensemble prediction: the RMSE measures, in an average sense, the difference between the mean ensemble trajectory, and the ANCR shows the average correlation between the mean ensemble trajectory and the true data trajectory. RMSE = 0 and ANCR = 1 would correspond to a perfect prediction, and small RMSEs and large (close to 1) ANCRs are desired.

For our reduced model, we computed the RMSE and ANCR using ensembles of  $N_{\text{ens}} = 100$  trajectories with independent initial conditions. Fig. 6 (left) shows the RMSE and ANCR for a range of lead times. As expected, the RMSE increases with lead time, and consistent with Fig. 1(a), it is relatively small compared to its apparent asymptotic value (about 0.6) for lead times  $< 50$ . The ANCR in Fig. 6 (right) corroborates this. The two figures are comparable to Fig. 5 of [36] and show very similar trends.

*Role of the noise terms  $\xi_n$ .* We experimented with running the reduced model with  $\xi_n \equiv 0$ , i.e., without any noise term. This does not appreciably change the ACF or marginal distributions, nor the forecasting skill of the reduced model. However, the kind of ensemble prediction and uncertainty quantification illustrated in Fig. 4 cannot be carried out without noise terms calibrated to the reduced model.

## B Stochastic Burgers equation

The nonlinear terms  $\{\Psi_{n-j}\}$  in Eq. (5.6c) are defined by

$$\Psi_{n-j}^a = u^{n-j}, \quad \Psi_{n-j}^b = R^{\Delta t}(u^{n-j}), \quad \text{and} \quad \Psi_{n-j,k}^c = \sum_{\substack{|k-l| \leq K, K < |l| \leq 2K \\ \text{or } |l| \leq K, K < |k-l| \leq 2K}} \tilde{u}_l^{n-1} \tilde{u}_{k-l}^{n-j} \quad \text{for } k = 1, \dots, K,$$

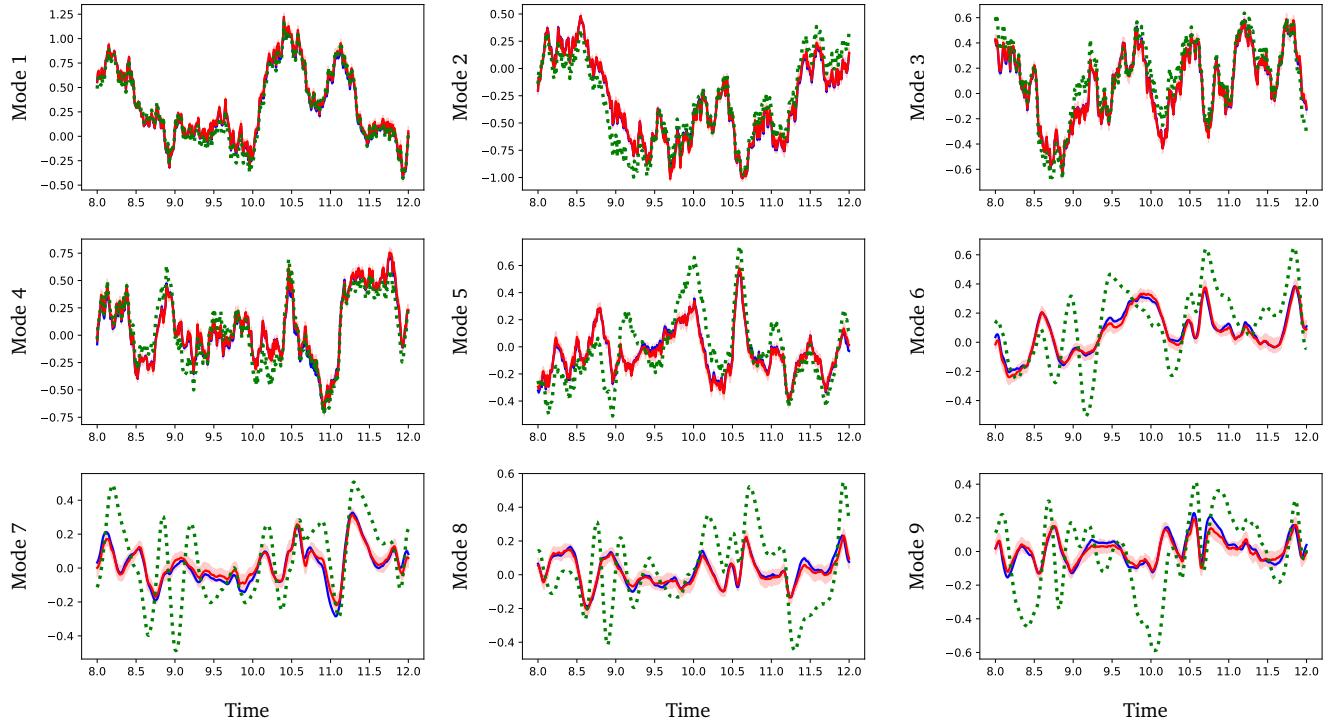


Figure 7: Response forecasting for the stochastic Burgers equation. For  $k = 1, \dots, 9$ , we plot  $\text{Re}(u_k(t))$  as functions of  $t$ . In all panels, solid blue line is the full model (128-mode truncation), dashed red line is the 9-mode reduced model, and dotted green line the 9-mode Galerkin truncation. Initial transients ( $t < 8$ ) are not shown.

where the terms  $\{\tilde{u}\}$  are defined as

$$\tilde{u}_k^{n-j} = \begin{cases} u_k^{n-j}, & 1 \leq k \leq K; \\ \frac{i\lambda_k}{2} e^{-\nu\lambda_k^2 j \delta} \sum_{\substack{|l| \leq K, \\ |k-l| \leq K}} u_{k-l}^{n-j} u_l^{n-j}, & K < k \leq 2K. \end{cases} \quad (\text{B.1})$$

These terms resemble those in Eq. (A.1d) as they are also introduced to represent the high modes by the low modes. But there is a major difference: they represent the high modes as a functional of the history of the low modes, rather than a function of the current state of the low modes. This is due to the lack of an inertial manifold for the Burgers equation, unlike the KSE. These terms are derived from a Riemann sum approximation of the integral equation for the high modes, with suitable linear parametrization of the quadratic interaction. A detailed derivation of the ansatz is presented in a forthcoming paper.

Figs. 7–10 show numerical results for the stochastic Burgers equation.

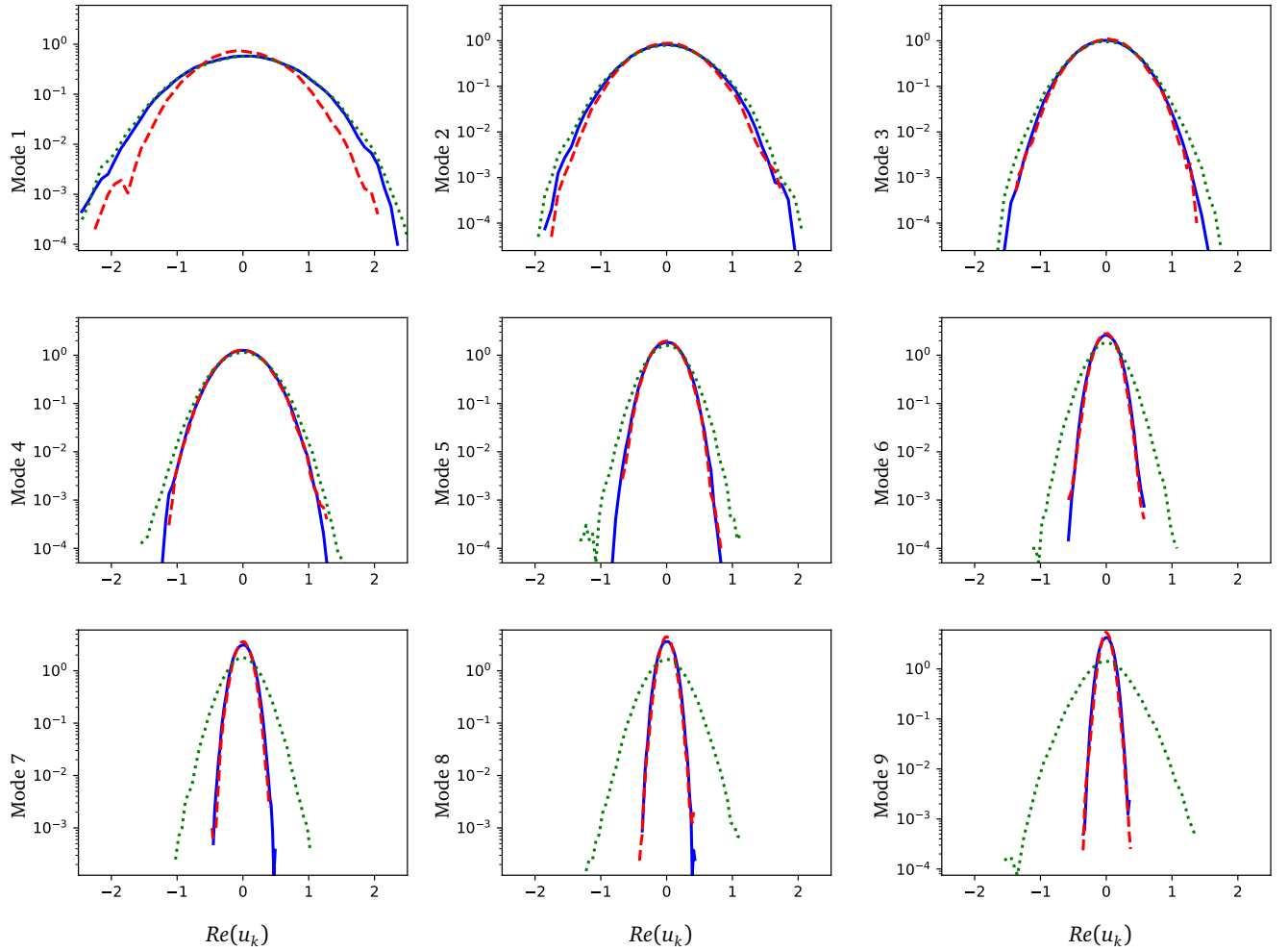


Figure 8: Marginal densities for the stochastic Burgers equation. We plot estimated densities for  $Re(u_k)$  for  $k = 1, \dots, 9$ . In all panels, solid blue line is the full model (128-mode truncation), dashed red line is the 9-mode reduced model, and dotted green line the 9-mode Galerkin truncation.

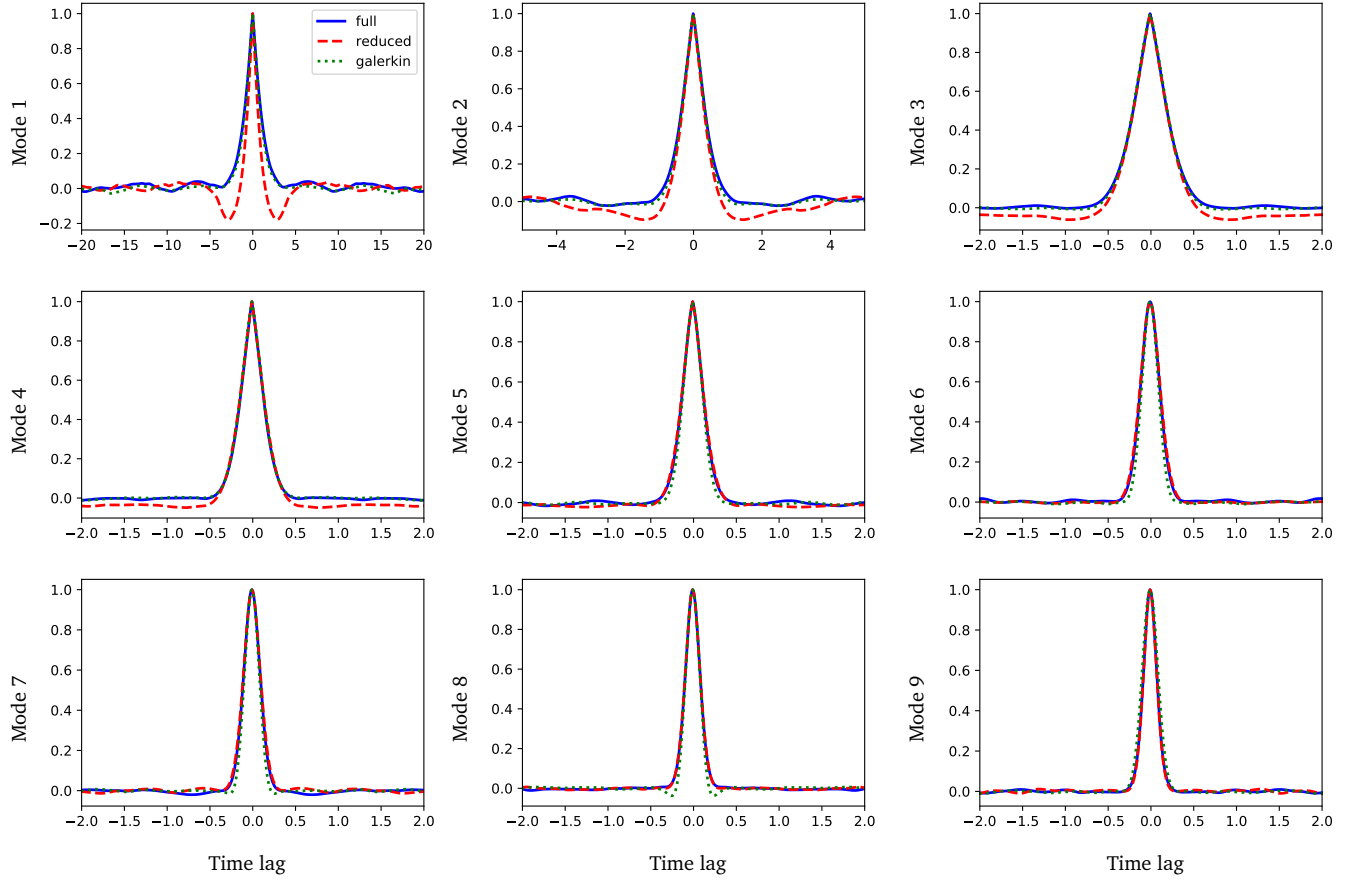


Figure 9: Autocorrelation functions for the stochastic Burgers equation. We plot autocovariance functions for  $Re(u_k)$  for  $k = 1, \dots, 9$ . In all panels, solid blue line is the full model (128-mode truncation), dashed red line is the 9-mode reduced model, and dotted green line the 9-mode Galerkin truncation.

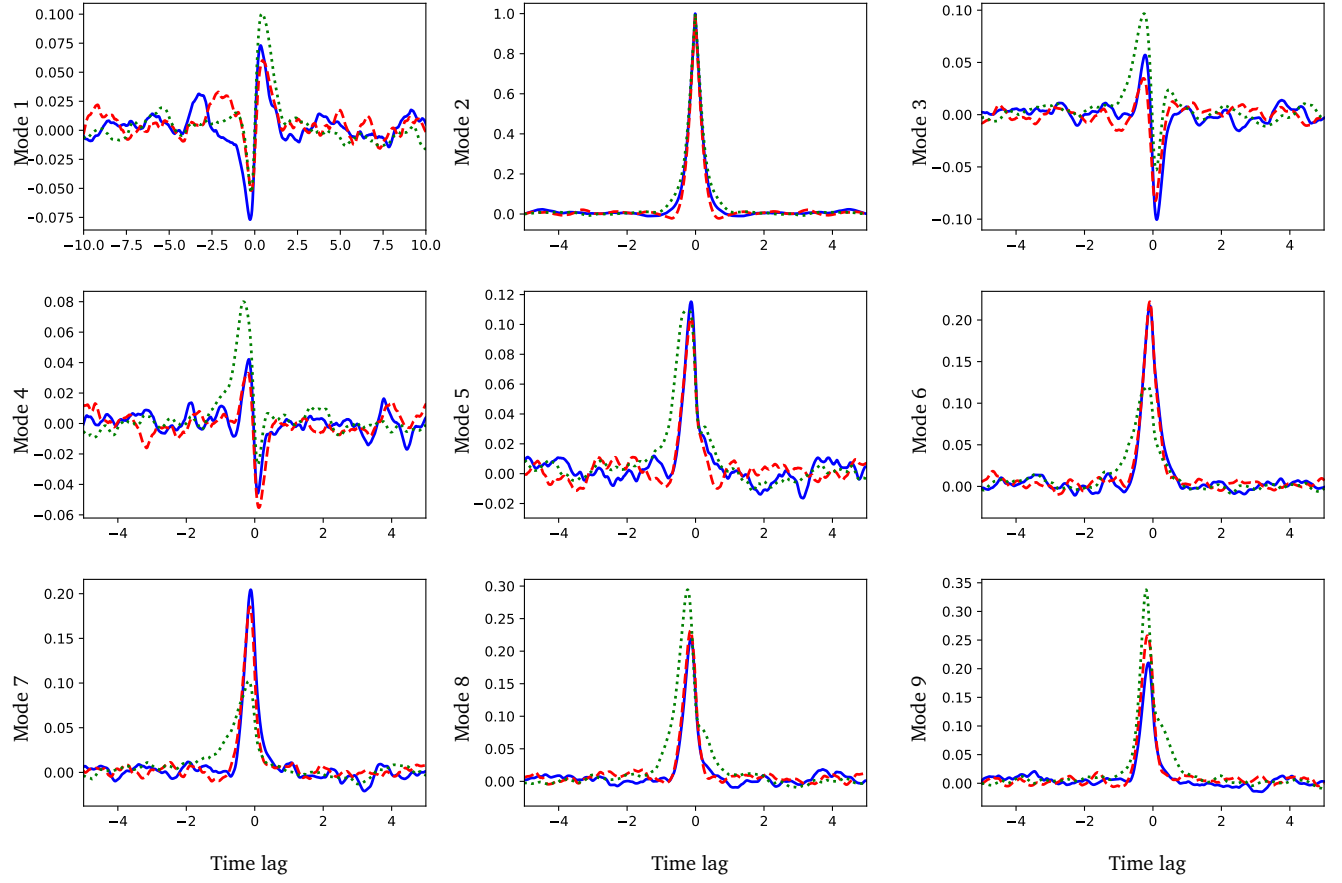


Figure 10: Energy cross-correlation functions for the stochastic Burgers equation. We plot cross correlation functions for  $|u_2|^2$  and  $|u_k|^2$  for  $k = 1, \dots, 9$ . In all panels, solid blue line is the full model (128-mode truncation), dashed red line is the 9-mode reduced model, and dotted green line the 9-mode Galerkin truncation.